The Astrophysical Journal, 649:129–149, 2006 September 20
© 2006. The American Astronomical Society. All rights reserved. Printed in U.S.A.

A SEARCH FOR LOW SURFACE BRIGHTNESS STRUCTURE AROUND COMPACT NARROW EMISSION LINE GALAXIES[1]

Elizabeth J. Barton,[2] Liese van Zee,[3] and Matthew A. Bershady[4]
Received 2006 April 6; accepted 2006 May 24

ABSTRACT

As the most extreme members of the rapidly evolving faint blue galaxy population at intermediate redshift, the compact narrow emission line galaxies (CNELGs) are intrinsically luminous ($-22 \lesssim M_B \lesssim -18$) with narrow emission line widths (30 km s$^{-1} \lesssim \sigma \lesssim 125$ km s^{-1}). Their nature is heavily debated: they may be low-mass starbursting galaxies that will fade to present-day dwarf galaxies or bursts of star formation temporarily dominating the flux of more massive galaxies, possibly related to in situ bulge formation or the formation of cores of galaxies. We present deep, high-quality ($\sim$0.″6–0.″8) images with CFHT of 27 CNELGs. One galaxy shows clear evidence for a tidal tail; the others are not unambiguously embedded in galactic disks. Approximately 55% of the CNELGs have sizes consistent with local dwarfs of small to intermediate sizes, while 45% have sizes consistent with large dwarfs or disk galaxies. At least four CNELGs cannot harbor substantial underlying disk material; they are low-luminosity galaxies at the present epoch ($M_B > -18$). Conversely, 15 are not blue enough to fade to low-luminosity dwarfs ($M_B > -15.2$). The majority of the CNELGs are consistent with progenitors of intermediate-luminosity dwarfs and low-luminosity spiral galaxies with small disks. CNELGs are a heterogeneous progenitor population with significant fractions (up to 44%) capable of fading into today's faint dwarfs ($M_B > -15.2$), while 15%–85% may only experience an apparently extremely compact CNELG phase at intermediate redshift but remain more luminous galaxies at the present epoch.

Subject headings: galaxies: evolution — galaxies: high-redshift

1. INTRODUCTION

Cosmological look-back time is one of the most powerful tools available to study galaxy evolution. To see the phases at which galaxies build their stellar populations rapidly, we look back in time to find dramatic starbursts. However, we must learn to identify the present-day galaxy population of which these starbursts are the progenitors. In this paper we work toward a broad understanding of the role of rapid star formation in the evolution of galaxies by investigating the nature of some of the most extreme starbursting galaxies at intermediate redshift, the compact narrow emission line galaxies (CNELGs). Although the CNELGs are rare in the intermediate-redshift universe ($\sim 7.5 \times 10^{-5}$ Mpc^{-3}; Koo et al. 1994), starburst timescales are much less than a Hubble time. Thus, starbursting galaxies may have a relatively low space density even if most galaxies go through such a phase.

Originally defined as stellar in ground-based images of moderate resolution ($\sim$1.″4 $\pm$ 0.″05 FWHM), CNELGs are intrinsically luminous star-forming galaxies ($-22 \lesssim M_B \lesssim -18$) with extremely small half-light radii (1 kpc $\lesssim R_e \lesssim$ 5 kpc) and narrow emission line widths in integrated spectra (28 km s$^{-1} \leq \sigma \leq 126$ km s^{-1}; Koo et al. 1995; Guzmán et al. 1996). The small sizes and narrow emission lines of these galaxies led Koo et al. (1995) to identify the CNELGs as possible starbursting objects that will fade by many magnitudes to become present-day low-luminosity dwarf elliptical (dE) galaxies. However, these authors also note an alternative explanation: that CNELGs are starbursts embedded in more massive galaxies, surrounded by an old stellar population. The two CNELGs with detailed abundance measurements in the literature are more metal enriched in their gas phase than the mean stellar metallicities of dwarf galaxies (Kobulnicky & Zaritsky 1999), potentially supporting this hypothesis as we consider further in § 3.2.1. In addition, kinematic line widths can underrepresent the masses of compact galaxies (Kobulnicky & Gebhardt 2000; Barton & van Zee 2001; Pisano et al. 2001). If CNELGs are starbursts embedded in more massive galaxies, they may be building stellar mass in central components such as bulges or cores forming in situ (Kobulnicky & Zaritsky 1999; Hammer et al. 2001). They may represent the formation of a separate class of bulges known as "pseudobulges" or "exponential bulges" that have properties consistent with in situ formation from the infall of disk gas and subsequent central formation (e.g., Carollo 1999; Kormendy & Kennicutt 2004).

High-resolution images of the CNELGs with the *Hubble Space Telescope* (*HST*) reveal lumpy high surface brightness structures within the starbursts in many cases (Guzmán et al. 1998). However, the lack of sensitivity to lower surface brightness features could hamper efforts to find older stellar populations in which CNELGs might be embedded.

Here we present deep ground-based imaging designed to observe the low surface brightness flux distribution of CNELGs. To interpret the data, the approach we take is to compare the properties of CNELGs to the various specific models of the nature of CNELGs, focusing on one in which they are dwarf elliptical galaxies undergoing a period of rapid star formation and one in which they are starbursts in the centers of galactic disks. In § 2 we describe the CNELG sample and the data reduction. Section 3 is a detailed comparison of the CNELG surface brightness distributions to starbursting dwarfs, disk galaxies, elliptical galaxies, and

[1] Based on observations obtained at the Canada-France-Hawaii Telescope, which is operated by the National Research Council of Canada, the Institut National des Sciences de l'Univers of the Centre National de la Recherche Scientifique of France, and the University of Hawaii.

[2] Center for Cosmology, Department of Physics and Astronomy, University of California, 4129 Reines Hall, Irvine, CA 92697-4575; ebarton@uci.edu.

[3] Department of Astronomy, Indiana University, 727 East 3rd Street, Bloomington, IN 47405; vanzee@astro.indiana.edu.

[4] Department of Astronomy, University of Wisconsin, 475 North Charter Street, Madison, WI 53706; mab@astro.wisc.edu.

TABLE 1
THE CNELGs

Field (1)	ID (2)	R.A. (J2000.0) (3)	Decl. (J2000.0) (4)	z (5)	z Quality (6)	m_R (7)	M_B (8)	$(B-V)_0$ (9)	$-\Delta m_{\max}$ (mag) (10)	σ (km s^{-1}) (11)	Exposure (ks) (12)	Notes (13)
SA 57	111867	13 07 14.0	+29 25 28	0.160	Q1	19.85	−18.8	0.35	1.7(2.5)	...	25.8	NGC 205
SA 57	111255	13 07 28.3	+29 24 40	0.180	Q3	21.78	−17.2	0.16	2.7(6.1)	...	25.8	NGC 205
SA 68	208846	00 16 31.1	+15 52 20	0.242	Q1	21.14	−18.5	0.32	2.3(3.0)	...	21.0	NGC 205
SA 57	112259	13 07 15.0	+29 26 03	0.252	Q3	21.06	−18.7	0.33	2.3(3.1)	...	25.8	NGC 205
SA 68	212668	00 18 04.9	+15 58 17	0.260	Q1	20.15	−19.6	0.38	2.2(2.9)	...	21.0	LARGE
SA 68	217054	00 17 40.8	+16 06 56	0.284	Q1	20.65	−19.3	0.41	2.1(2.9)	...	21.0	INTERMED
SA 68	206134	00 18 11.3	+15 47 54	0.285	Q1	20.29	−19.8	0.27	2.6(3.6)	41[a]	21.0	VCC 437
SA 68	203307	00 16 55.0	+15 43 06	0.297	Q1	20.59	−19.5	0.35	2.4(3.1)	...	21.0	INTERMED
SA 57	108954	13 09 35.7	+29 21 16	0.319	Q1	20.47	−19.9	0.17	3.2(6.2)	...	25.8	VCC 437
SA 68	217255	00 17 22.9	+16 07 26	0.348	Q1	19.40	−21.2	0.31	2.7(3.4)	40[a]	21.0	LARGE
SA 68	217169	00 16 56.2	+16 07 11	0.354	Q1	21.28	−19.3	0.32	2.6(3.4)	...	21.0	NGC 205
SA 68	217779	00 16 49.1	+16 08 47	0.377	Q3	21.18	−19.6	0.40	2.4(3.2)	...	21.0	INTERMED
SA 68	212916	00 16 28.9	+15 58 46	0.418	Q1	20.54	−20.5	0.41	2.5(3.2)	...	21.0	VCC 437
SA 57	112536	13 09 06.8	+29 26 32	0.420	Q1	21.07	−20.0	0.32	2.8(3.5)	...	25.8	INTERMED
SA 57	110601	13 08 47.7	+29 23 41	0.438	Q1	20.70	−20.5	0.18	3.5(6.4)	43[b]	25.2	VCC 437
SA 57	108956	13 09 48.2	+29 21 15	0.439	Q2	20.91	−20.3	0.26	3.1(4.5)	...	25.8	LARGE
SA 57	105482	13 09 08.7	+29 15 57	0.453	Q1	20.43	−20.8	0.36	2.7(3.5)	60[b]	25.8	INTERMED
SA 68	206403	00 17 17.6	+15 48 20	0.468	Q1	20.55	−20.8	0.40	2.6(3.4)	...	21.0	NGC 205
SA 68	215428	00 18 06.2	+16 03 17	0.482	Q2	20.60	−20.9	0.42	2.5(3.3)	...	21.0	VCC 437
SA 68	216388	00 18 16.5	+16 05 11	0.488	Q1	20.31	−21.2	0.43	2.5(3.2)	...	21.0	VCC 437
SA 57	117671	13 07 31.7	+29 34 33	0.518	Q2	21.07	−20.6	0.44	2.5(3.1)	...	25.8	INTERMED
SA 57	107042	13 07 26.2	+29 18 24	0.525	Q1	21.41	−20.3	0.36	2.8(3.6)	116[b]	25.2	VCC 437
SA 68	217418	00 17 45.3	+16 07 47	0.553	Q1	21.20	−20.7	0.30	3.0(3.8)	...	21.0	LARGE
SA 57	118170	13 07 38.8	+29 35 26	0.586	Q2	21.30	−20.8	0.35	2.9(3.7)	...	25.8	INTERMED
SA 57	108945	13 08 37.8	+29 21 15	0.608	Q2	21.31	−20.9	0.39	2.8(3.6)	...	25.8	INTERMED
SA 57	117731	13 08 38.2	+29 34 48	0.663	Q1	20.65	−21.8	0.31	3.1(3.9)	103[b]	25.8	VCC 437
SA 68	209640	00 17 55.3	+15 53 30	0.728	Q1	21.48	−21.4	0.39	2.9(3.7)	...	21.0	NGC 205
Compact Galaxies												
SA 68	205935	00 17 41.2	+15 47 36	0.304	Q1	20.45	−19.8	0.27	2.7(3.6)	...	21.0	LARGE
SA 57	103605	13 07 53.0	+29 12 53	0.392	Q1	21.23	−19.6	0.34	2.7(3.4)	37[b]	25.2	LARGE
SA 57	104259	13 08 03.4	+29 14 00	0.601	Q1	21.01	−21.2	0.38	2.8(3.6)	52[b]	25.8	LARGE

NOTES.—Basic properties of the final sample of CNELGs and compact galaxies. Col. (1): Field. Col. (2): ID number from the original study. Cols. (3) and (4): J2000.0 coordinates; units of right ascension are hours, minutes, and seconds, and units of declination are degrees, arcminutes, and arcseconds. Col. (5): Redshift. Col. (6): Quality of redshift information: Q1 = high-quality redshift; Q2 = one-line identification; Q3 = low-quality redshift. Col. (7): Measured R-band apparent magnitude. Col. (8): Computed rest-frame B-band absolute magnitude. Col. (9): Computed rest-frame $B-V$ color. Col. (10): Maximum fading in magnitudes of the CNELG to the present day corresponding to the $B-V$ color without (with) reddening correction and look-back time (see § 3.1.1). Col. (11): Emission-line velocity dispersion from the literature. Col. (12): Imaging exposure time in R for this study. Col. (13): Classification from § 3.1: NGC 205 = like NGC 205; INTERMED = between NGC 205 and VCC 437; VCC 437 = like VCC 437; LARGE = larger than VCC 437 (disk galaxy–like).

[a] Guzmán et al. (1996).

[b] Koo et al. (1995).

E+A galaxies. In §§ 4 and 5 we discuss the results and list our conclusions. We adopt a cosmology in which $\Omega_\Lambda = 0.7$, $\Omega_m = 0.3$, and $H_0 = 70$ km s^{-1} Mpc^{-1}.

2. THE SAMPLE AND DATA REDUCTION

We study a subset of CNELGs that have existing Keck spectroscopy in the literature. The parent sample originates from the photographic plate study of Kron (1980), including the fields SA 57 and SA 68 observed to 50% completeness depths of $B_J \sim 23$ and $R_F \sim 22$ (see Kron 1980; Koo 1986; Koo & Kron 1988; Munn et al. 1997). We reobserve the fields in the R band for 6–7 hr in queue mode with the 12k camera at the Canada-France-Hawaii Telescope (CFHT) during optimal seeing conditions (Martin et al. 2002). The new data are roughly 10 times deeper, with roughly half the seeing disk of the original plate observations.

We exclude objects from the analysis that are too close to the edges of the detector, galaxies that are next to very bright stars, and one unresolved galaxy with low-quality spectroscopy that would be much too intrinsically luminous at its tentative redshift. The final sample of observed galaxies includes 27 CNELGs and three additional compact galaxies. Of the 27 CNELGs, 19 have high-quality redshift identifications, 5 have one-line redshifts, and 3 have low-quality redshifts.

The deep R-band images of the CNELGs are dithered pointings of 600 s duration spread over several nights. We list the total exposure times of high-quality data for each object in Table 1. The seeing FWHM of the final combined images ranges from $\sim$0.″6 to 0.″8. The preliminary data reduction was conducted with the Elixir pipeline processing software at CFHT (Magnier & Cuillandre 2004). Nominally, the flat fields allow photometric accuracy to $\sim$2%. The photometric solutions provided by Elixir were verified by comparing the new results with previous observations of these objects. Further, for SA 57, we recomputed the photometric solutions by comparing with R-band data in Majewski et al. (1994). While there was good agreement with the Elixir results, we use the revised calibration for the object

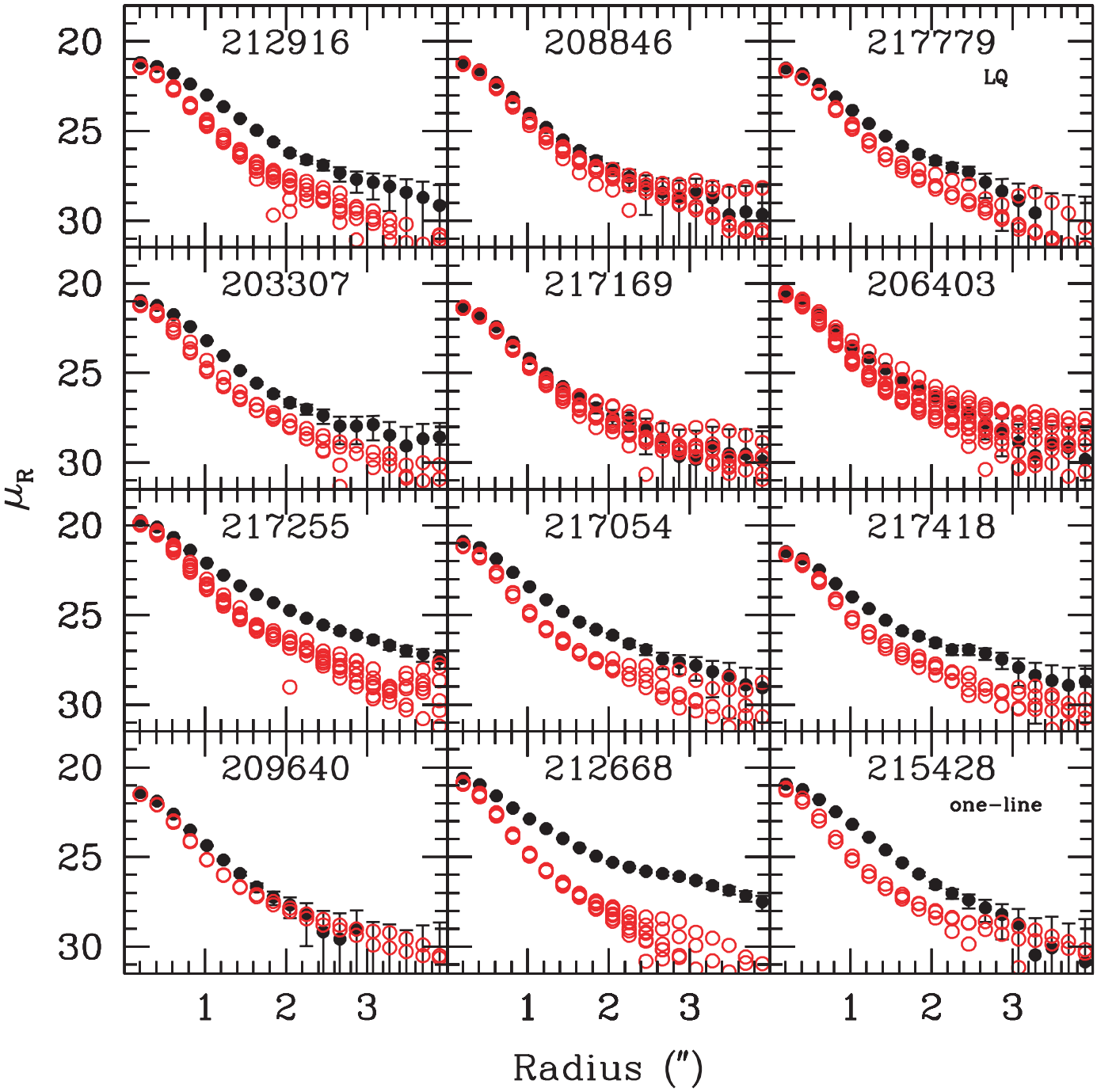

FIG. 1.—*R*-band circular aperture surface brightness profiles of the CNELGs. The open circles show the PSF from profiles of nearby stars scaled to the central surface brightness of the CNELG. Labels are as follows: *one-line*: one-line spectroscopic redshifts; *LQ*: low-quality spectroscopic data; *extended*: extended source in original imaging data (not a CNELG).

photometry we present for this field. Our postprocessing with the MSCRED package in IRAF[5] includes coordinate solutions, image projection, and combination. Finally, we subtract the background using a large mesh size with SExtractor (Bertin & Arnouts 1996). The typical 1 σ surface brightness limits for the combined images are $\sim$28 mag arcsec^{-2}.

Table 1 lists the basic properties of the sample. We use the measured m_R from our data but construct rest-frame $B - V$ colors and M_B from a compilation of the photographic B_J and R_F magnitudes and spectroscopic redshifts: from the Munn et al. (1997) study for the three "compact galaxies," from the series of papers on deep QSO surveys in SA 57 and SA 68 (Koo et al. 1986; Koo & Kron 1988; Trevese et al. 1989, 1994; Bershady et al. 1998) for most of the CNELGs in SA 57, and from previously unpublished catalogs related to the Munn et al. (1997) survey for the remainder. We use the transformations from Majewski (1992) to convert observed $B_J - R_F$ to observed $B - V$, noting that these transformations are strictly relevant to stellar spectral energy distribution (SED) in the rest frame. Using galaxy SED templates from Coleman et al. (1980) and a starburst template from Bruzual

[5] IRAF is distributed by the National Optical Astronomy Observatory, which is operated by the Association of Universities for Research in Astronomy, Inc., under cooperative agreement with the National Science Foundation.

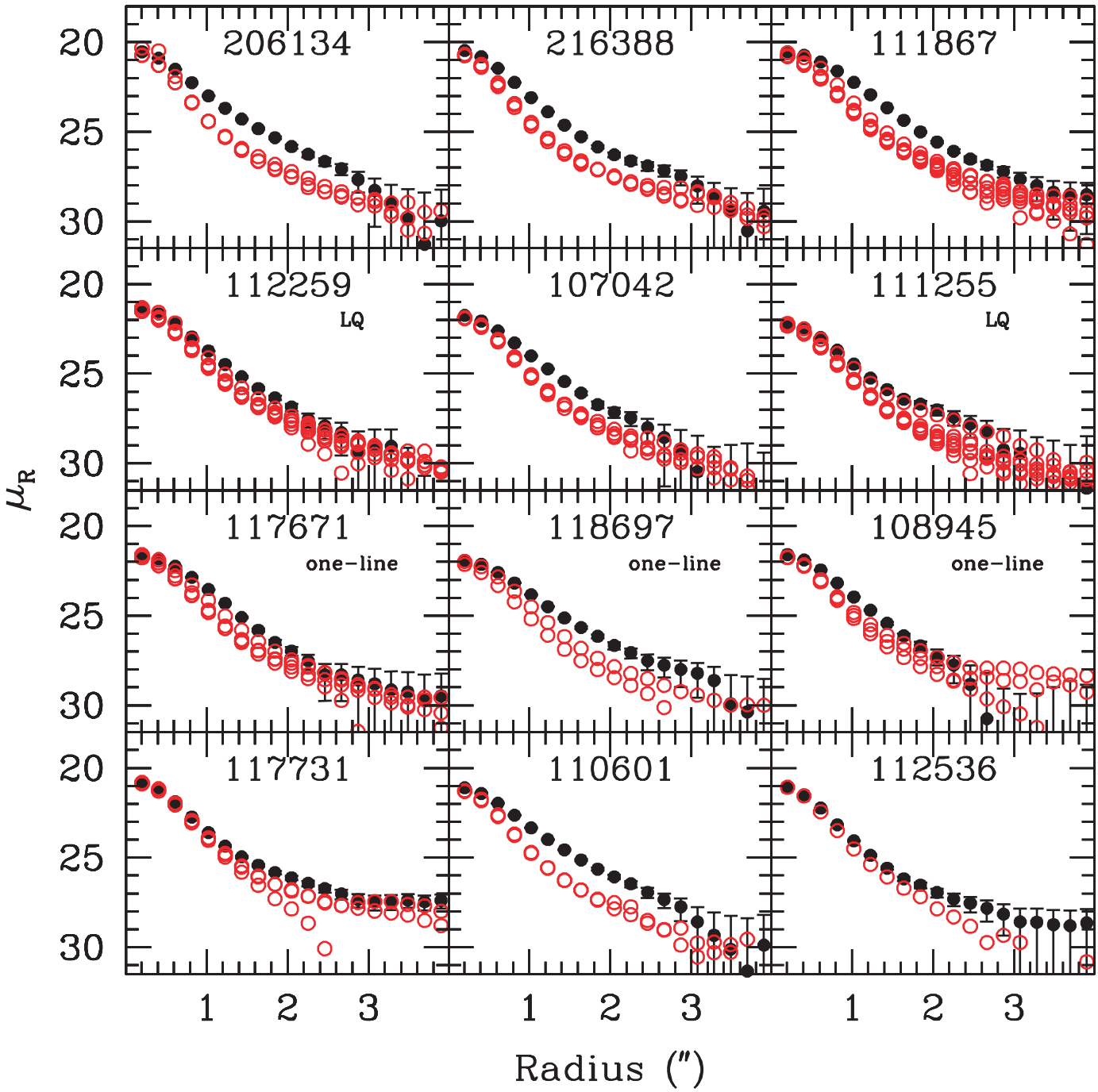

FIG. 1.—*Continued*

& Charlot (2003), we interpolate between templates to match the observed-frame $B - V$ colors and use the interpolated templates to derive rest-frame $B - V$ colors and M_B. A comparison between rest-frame $B - V$ calculated here and in Guzmán et al. (1998) yields the same mean values for eight objects, but a significant dispersion of 0.1 mag.[6] We adopt this as an estimate of the uncertainty in deriving rest-frame colors, which comes into play when we discuss the possible fading of these sources in § 3.1.1.

[6] The Guzman et al. (1998) study uses the same redshifts but includes the photographic U and I_N bands, and in some cases this was augmented by *HST* WFPC2 $V_{606} - I_{814}$ colors in their analysis.

2.1. *Surface Brightness Distributions of the Compact Narrow Emission Line Galaxies*

Figure 1 shows the surface brightness profiles of the final sample (*filled circles*) based on circular aperture photometry with SExtractor; the smaller open circles are the profile(s) of a nearby star(s) scaled to the central surface brightness of the CNELG. Several CNELGs are unresolved or very nearly unresolved in the images. As we demonstrate below, most of these unresolved galaxies are probably intrinsically small objects. Figure 2 shows contour plots of the CNELGs. The CNELGs are clearly a heterogeneous population of objects. Many of the CNELG profiles resemble the stellar profiles in the inner regions, suggesting that the inner parts of the galaxies are largely unresolved. Therefore, the

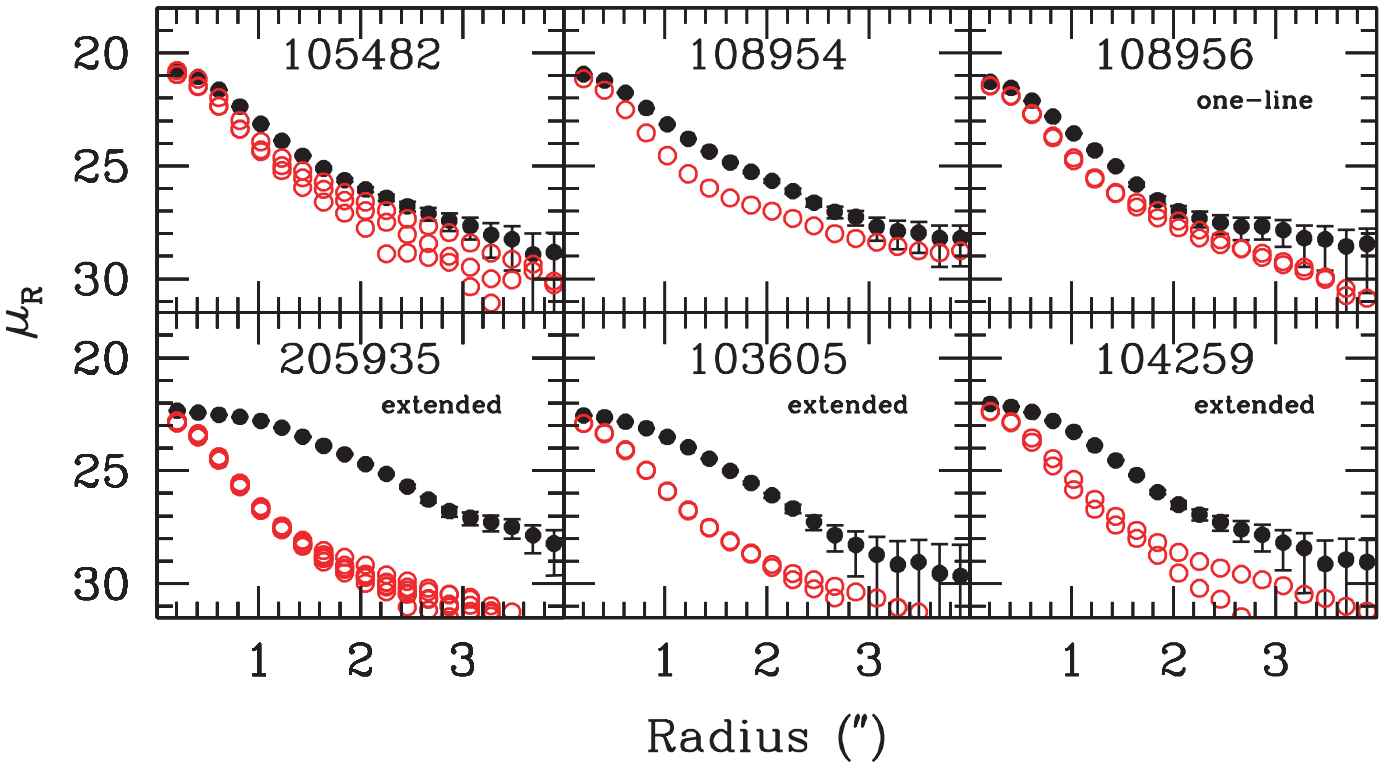

FIG. 1.—*Continued*

sensitivity of our imaging observations to detect underlying disks relies on the analysis of the faint outskirts of the galaxies, where the depth of our observation must be combined with careful data reduction and modeling to determine the types of extended flux to which we are sensitive.

Background galaxies have a large filling factor in deep images of the universe. A superposition of a CNELG on a low surface brightness background (or foreground) galaxy could lead to the misidentification of structure in the outskirts of the CNELG. We use a simple Monte Carlo simulation to explore the probability that this effect is significant. The superposition would not be evident in even high-quality spectra because the high surface brightness CNELG dominates the flux. We add 16 flux-boosted, artificially redshifted versions of NGC 205 (see § 3.1) to randomly drawn positions in the images and count the objects that deviate from the profile of a simulation added to blank sky. We do not count obvious superpositions where the "artificial CNELG" (NGC 205) is separated from an adjacent but distinct object; we count only those that we would likely mistake for underlying structure. For 480 simulated fake CNELGs, we find an average rate of 23% for superpositions, where 15% are obvious superpositions that would probably never have been identified as CNELGs. Of the remaining CNELG simulations, 8.6% are accidental superpositions that would not have been obvious. Thus, our analysis must allow for the fact that on average we expect that 2.3 ± 1 of the 27 CNELGs are superpositions on extended, low surface brightness background galaxies.

3. SCENARIOS FOR THE NATURE OF THE CNELGs

The defining characteristics of CNELGs are their extremely compact sizes yet large blue luminosities, blue optical colors, and strong and narrow line emission. Studies of these objects and of similar luminous compact blue galaxies reveal a heterogeneous population of objects including some that probably fade to become dwarfs and some star-forming disk galaxies that fade to become luminous but sub-L^* systems, just below the "knee" in the luminosity function. They exhibit a range of emission-line widths, a range of stellar masses based on modeling of near-infrared fluxes, and a range of morphologies (Koo et al. 1994, 1995; Guzmán et al. 1996, 1997, 1998, 2003; Phillips et al. 1997; Hammer et al. 2001). Here we scrutinize the surface brightness profiles of the CNELG population from the SA 57 and SA 68 fields, comparing their surface brightness profiles and colors to models based on the hypotheses that some CNELGs are bursting dwarf galaxies, starbursts in the center of disk galaxies (possibly galactic bulges in formation), the cores of elliptical galaxies in formation, and/or the progenitors of E+A galaxies, which are galaxies with strong post-starburst spectra.

3.1. *The Bursting Dwarf Hypothesis*

The bursting dwarf hypothesis posits that the luminous, compact star-forming galaxies observed at intermediate redshift are the progenitors to local dwarf galaxies. In this scenario, the distant bursting dwarfs deplete their gas reservoirs in a violent burst of star formation, fading to become the dwarf elliptical galaxies (dEs) observed in abundance in the local universe. This interpretation of the CNELGs is compelling because their emission-line widths and sizes are appropriate for dwarfs and not for more luminous galaxies (e.g., Guzmán et al. 1996). Here we begin with the model that CNELGs actually are dEs during a bursting phase and test the consistency of that picture.

Formed stellar populations generally cannot shrink in size with time. Thus, if CNELGs are starbursting dwarf galaxies that ultimately fade to become dwarfs in the local universe, the sizes of CNELGs are probably similar to or smaller than their counterpart dwarfs in the local universe. Supporting this conclusion,

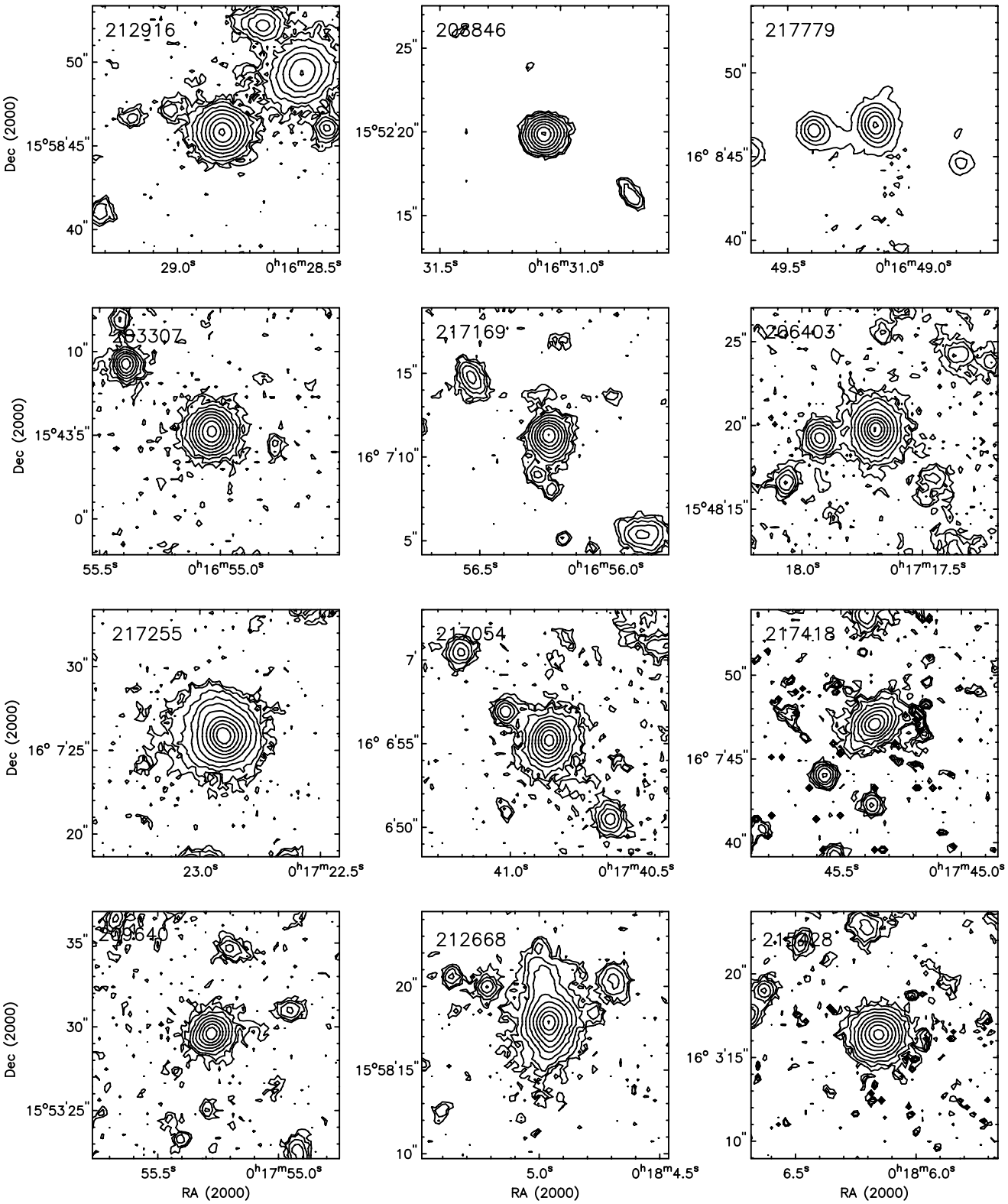

FIG. 2.—Logarithmic contour plots of the *R*-band images of CNELGs. The lowest contour corresponds to 27.3 mag arcsec^{-2} for all except 107042, 108945, 111255, 112259, 117731, 216388 (26.5 mag arcsec^{-2}), 110601, 117671 (25.8 mag arcsec^{-2}), and 217779 (25.3 mag arcsec^{-2}). In all cases, the contours are separated by 0.75 mag arcsec^{-2}.

the CNELGs themselves are observed to have radial color gradients (Guzmán et al. 1998), typically with blue cores. If CNELGs fade to dEs, the aging stellar populations in local dEs do not contradict the conclusion that they do not shrink with time. In particular, dEs exhibit only mild systematic gradients in color or stellar population (e.g., Vader et al. 1988; Jerjen et al. 2000; Barazza et al. 2003; van Zee et al. 2004a); if anything, most are slightly ($\sim$0.1 mag) redder in their centers than their outskirts. Therefore, we assume that CNELGs are smaller than or equal to the sizes of the objects to which they ultimately fade.

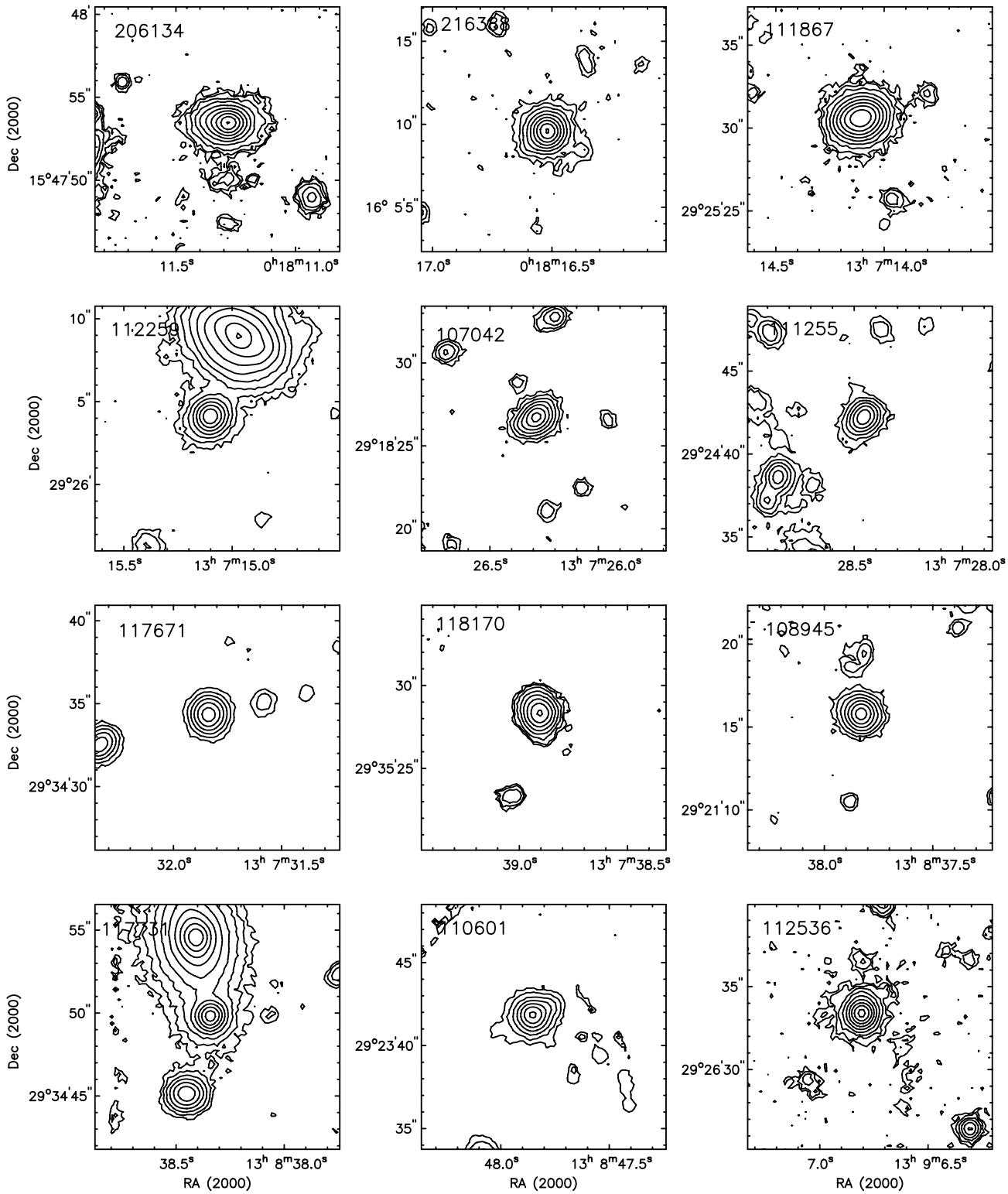

FIG. 2.—*Continued*

To test the hypothesis that CNELGs are the progenitors of dwarfs, we compare their sizes directly to examples of both compact and more extended local dEs. We use this analysis to argue that objects that are larger than dEs do not fade to become dEs by the present epoch, taking examples from a wide range of small and large dEs. The fiducial example of a small dwarf CNELG analog is NGC 205, a dwarf companion to M31. The Virgo Cluster holds a more varied population of dEs, including galaxies that are much larger than NGC 205. Figure 3 shows the central surface brightnesses and scale lengths of NGC 205[7] and a

[7] Observations of NGC 205 were obtained with the Mosaic camera on the WIYN 0.9 m telescope on 2003 December 19. The observations consisted of three 300 s exposures in the *B* band; the observations were dithered substantially to fill in the interstitial gaps. While the night was nonphotometric, photometric calibration was obtained by comparison with the integrated magnitudes tabulated in Mateo (1998).

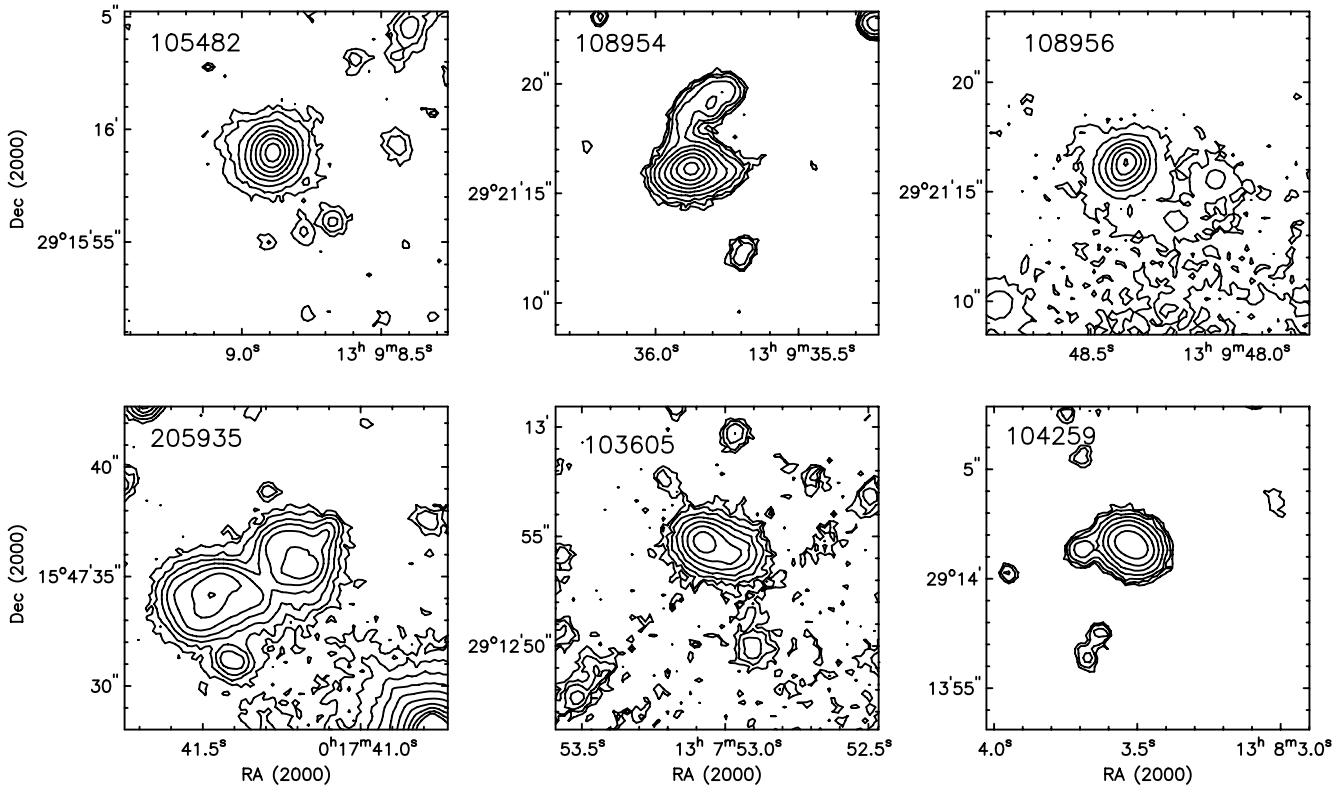

FIG. 2.—*Continued*

set of Virgo dEs (van Zee et al. 2004a). The shaded regions show the half-width at half-maximum (HWHM) of the range of seeing disks in the CFHT data at different redshifts. Although this figure serves as a guide to the sizes of these objects, whether or not we can resolve these objects depends on their luminosities and surface brightness profiles. We explore these questions in more detail below, using simulations added to the data.

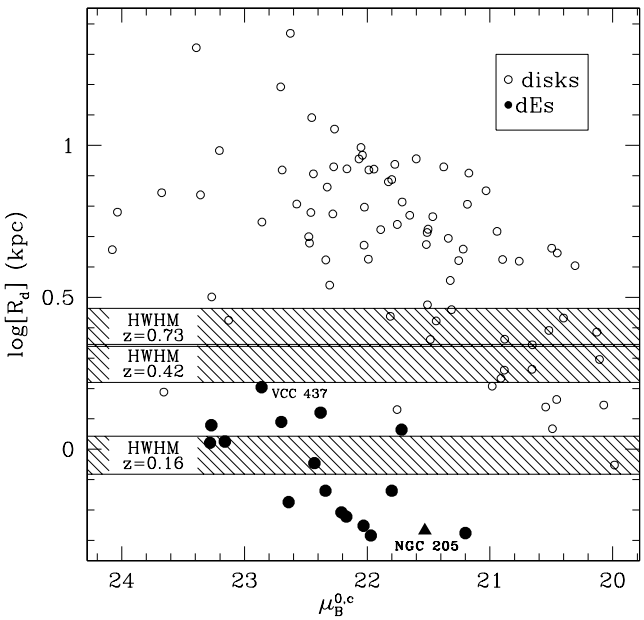

FIG. 3.—Structural parameters for Virgo dEs (*filled circles*) from van Zee et al. (2004a), for NGC 205 (*filled triangle*), and for local disks (*open circles*) from de Jong (1996). We plot the log of the half-light radii of the galaxies as a function of the disk rest-frame *B*-band central surface brightness. We shade the HWHM of the typical stellar PSFs for our data (range 0″.6–0″.8) at different redshifts. Low-luminosity dwarfs would be barely resolved or unresolved, except at the lowest redshifts; the larger dwarfs and most disks would be resolved.

Using a rest-frame *B*-band image of NGC 205 from the WIYN 0.9 m telescope and *B*-band images of elongated Virgo dEs from van Zee et al. (2004a), we evaluate the bursting dwarf hypothesis by comparing the surface brightness profiles of CNELGs to artificially redshifted versions of dwarf galaxies. To construct the model bursting dwarfs, we boost the integrated flux of the model to the measured *R*-band apparent magnitude of the CNELG with which we are comparing. We recompute the physical scale of the image at the redshift of the CNELG and rebin the data to the 0″.205 resolution of the CFHT data. We convolve with the point-spread function (PSF) using a nearby star. We simulate the appropriate Poisson noise for the object flux and add the object to the frames near the relevant CNELGs. We measure surface brightness profiles with a procedure that is identical to that used for the CNELGs themselves.

Figures 4 and 5 show examples of the resulting boosted-dwarf surface brightness profiles. The red circles are nearby stars boosted to match the central surface brightness of the CNELG or artificial dwarf. Figure 4 includes examples at the highest and lowest redshifts of the sample (111867 and 209640, respectively), as well as 212916 at the median redshift, $z = 0.42$. The figures highlight the fact that our discriminatory power varies as a function of redshift. For example, our data resolve NGC 205 at $z = 0.16$, but it is essentially unresolved at $z = 0.73$. However, we would be able to resolve VCC 437 at any redshift in our range.

In Figure 4, 111867 and 209640 are similar to NGC 205, but the remaining galaxies are larger or have detected flux extending to larger radii. Figure 5 shows that 212668 is more extended than even our model version of the largest Virgo dE from van Zee et al. (2004a), VCC 437, viewed as though it were a face-on disk. It has an exponential scale length of $R_d = 1.6$ kpc that is large enough to fall within the size range of small disk galaxies. Similar

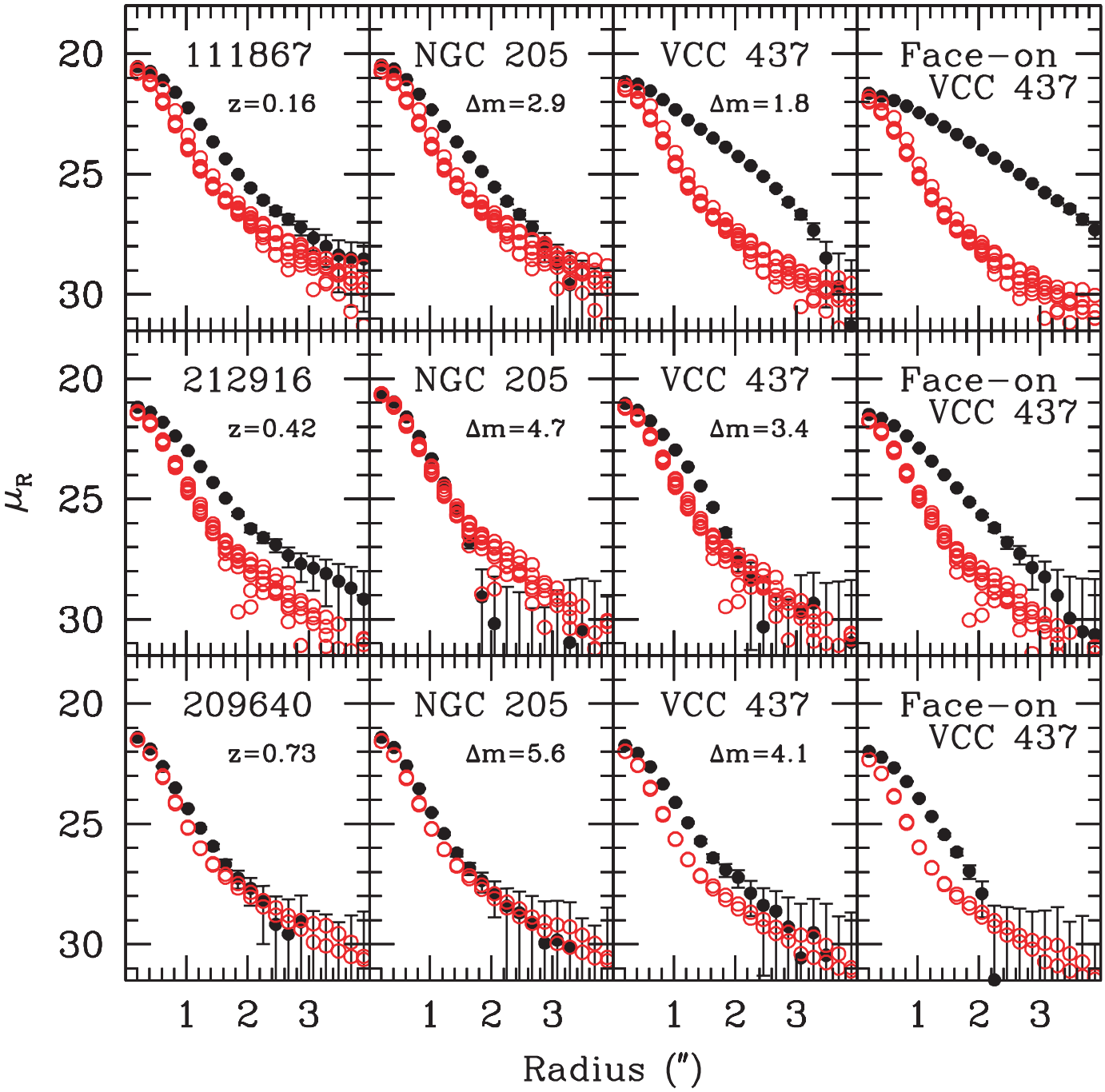

FIG. 4.—Comparing compact CNELGs to models of artificially redshifted dwarf galaxies. In each row, we plot the circular aperture surface brightness profile of a CNELG (*left, black*), labeling the plot with the ID number and redshift. The remaining three columns, from left to right, are (1) an artificially redshifted version of NGC 205 at the redshift of the CNELG with a magnitude boost given by Δm; (2) an artificially redshifted VCC 437, the largest dwarf in the van Zee et al. (2004a) sample of elongated Virgo dEs, with a scale length of $R_d = 1.6$ kpc; and (3) an artificially redshifted "face-on" model version of VCC 437 that is an exponential disk with the scale length and central surface brightness of VCC 437. In each panel we plot surface brightness profiles of nearby stars scaled to the central surface brightness of the object (*red*). NGC 205 is only resolvable at the lowest redshifts; most of the other Virgo dEs are barely resolved, except those with long disk scale lengths. In contrast, most known galactic disks would be resolved.

figures for the remaining galaxies indicate that of the CNELGs, 7/27 (26%) are smaller than or similar in size to NGC 205, 8/27 (30%) are between NGC 205 and VCC 437 and thus plausible typical dEs, 8/27 (30%) are similar in spatial extent to VCC 437 and thus consistent with a large dwarf or small spiral, and 4/27 (15%) are more extended than even the largest dE in the van Zee et al. (2004a) sample. We list these broad classifications in Table 1 and use them to group the CNELGs hereafter.

To compute the true amount of (integrated) B-band luminosity boost required to match the integrated R-band flux of the CNELG, we use the interpolated template SED corresponding to the rest-frame $B - V$ color of the CNELG to generate k-corrections for the hypothetical bursting dwarf (see § 2). For NGC 205, the required boosts range from 1.5 to 6.0 mag. The Virgo dEs fall into a more reasonable range. For the most luminous dE, VCC 1261, the required burst luminosity boosts satisfy $0.1 < \Delta m < 4.6$; for the

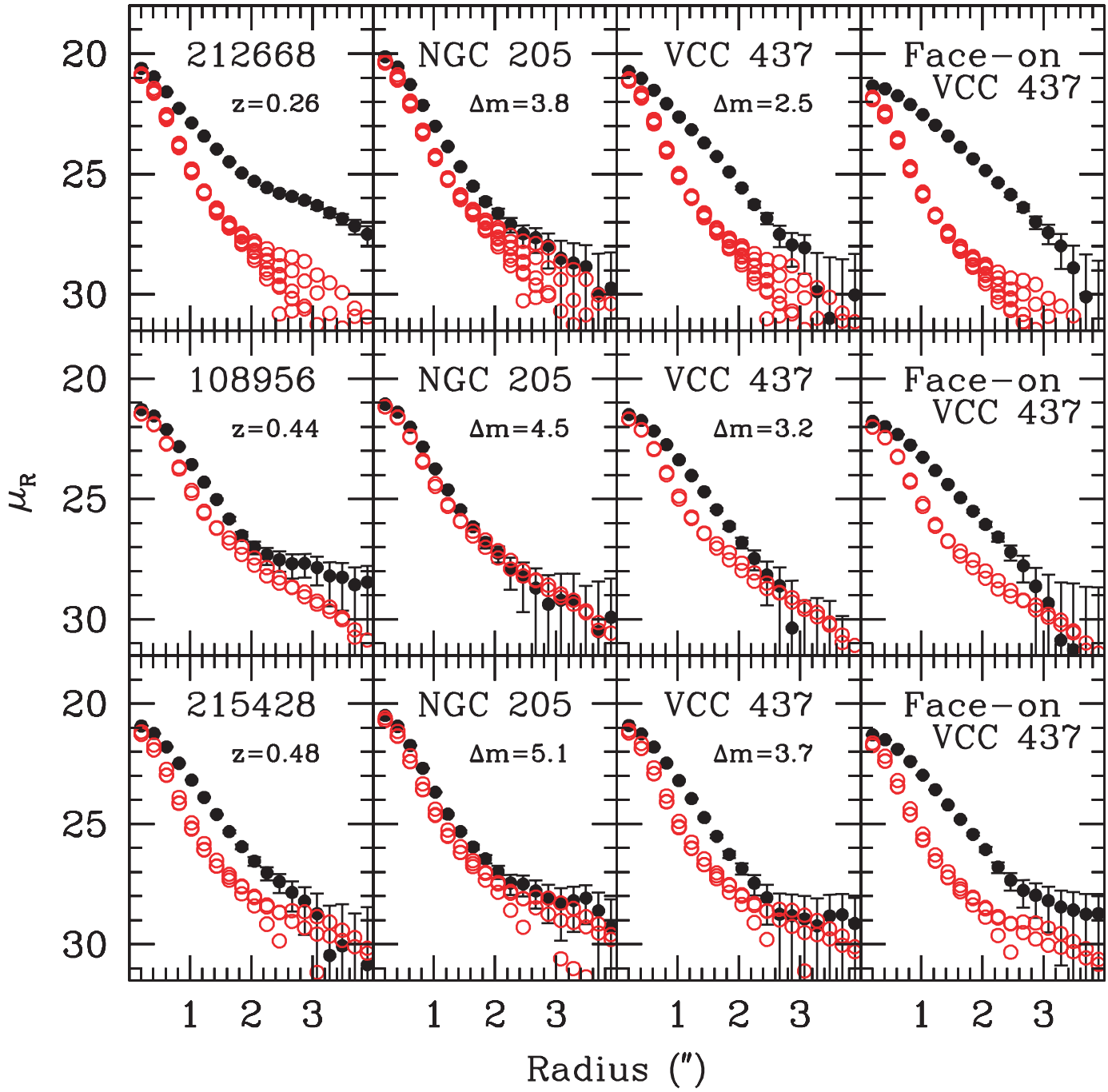

FIG. 5.—Same as Fig. 4, but for more extended CNELGs.

least luminous dE of the van Zee et al. (2004a) sample, the requirements are in the range $2.1 < \Delta m < 6.6$. Below we examine the constraints on luminosity fading for individual CNELGs available from their rest-frame colors.

3.1.1. *Fading Limits for the CNELGs*

Spectral synthesis models provide a means of estimating an upper limit to the amount that CNELGs have faded to the present day. Figure 6 shows the amount of fading and the composite colors for Bruzual & Charlot (2003) models with added starbursts. Adopting a Chabrier (2003) stellar initial mass function and solar metallicity, we assume two episodes of star formation that are bursts of equal duration. The second burst occurs 8 Gyr after the first with an amplitude of 0%, 1%, 50%, or 100%. On the plot, time is measured since the start of the second burst. More rapid bursts reach higher fractional peak luminosities.

For global bursts of star formation, the burst timescales must be greater than or similar to the dynamical timescales. With central velocity dispersions 25 km s$^{-1} \lesssim \sigma_0 \lesssim$ 50 km s^{-1} (Geha et al. 2003; van Zee et al. 2004b) and disk scale lengths 0.5 kpc $\lesssim \alpha^{-1} \lesssim$ 1.6 kpc (e.g., van Zee et al. 2004a), the dynamical timescales of the Virgo dEs are always $\gg$10 Myr and usually $\gtrsim$100 Myr. Thus, we consider models in which the bursts last 10 and 100 Myr as typical timescales for global starbursts in a dE. For comparison, estimated dynamical timescales for CNELGs yield a mean of 20 Myr within the half-light radius as observed at intermediate

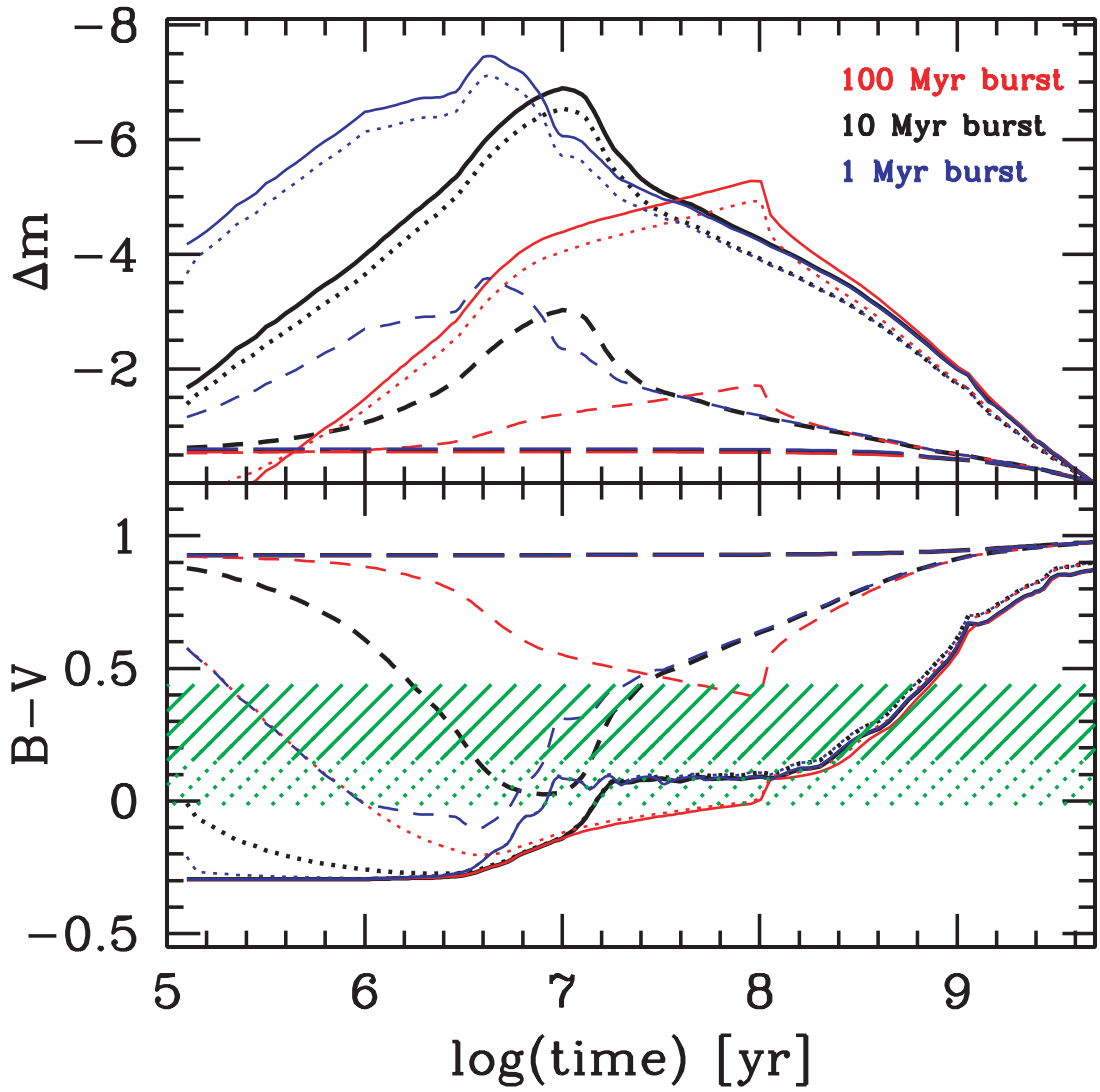

FIG. 6.—Starburst colors and fading limits from Bruzual & Charlot (2003) stellar spectral synthesis models. We plot the amount of fading (*top*) and the composite rest-frame $B - V$ color (*bottom*) for starbursts with amplitudes of 0% (*long-dashed line*), 1% (*short-dashed line*), 50% (*dotted line*), and 100% (*solid line*) for starbursts with constant star formation rates for 1 (*blue*), 10 (*black*), and 100 Myr (*red*). The shaded region indicates the observed color range in our sample. This color range corresponds to a maximum fading of ~3.5 mag in the 5 Gyr following the burst ($z = 0.5$).

redshift.[8] More localized bursts of star formation may last for shorter amounts of time. Thus, we include 1 Myr bursts to encompass this possibility. We note that abundance patterns in nearby dwarfs appear to rule out star formation histories that involve extremely rapid formation of ~100% of the stellar population: such a scenario would result in alpha-enhanced dwarfs, while dEs typically have solar or subsolar [α/Fe] ratios (Geha et al. 2003; van Zee et al. 2004a), indicating that their dominant stellar population was not formed in a single rapid starburst. In any case, we find that the derived fading limits are insensitive to choice of burst timescale in the explored range.

Our inability to correct for extinction accurately, on an object-by-object basis, is the most important systematic error of this analysis. The average measured $E(B - V)$, derived for seven CNELGs by Kobulnicky & Zaritsky (1999) and Hoyos et al. (2004), is 0.17. However, if the CNELGs are starbursting dwarfs that resemble strongly star-forming dwarfs in the nearby universe, their reddening may be minimal. Thus, we compute the expected fading of CNELGs assuming both no dust and $E(B - V) = 0.17$.

As Figure 6 shows, objects that will fade by $\gtrsim$3.5 mag ($\Delta m \leq -3.5$) in the 5 Gyr after the burst are bluer than the observed CNELGs for any of these scenarios, unless the rest-frame colors are corrected for dust. A correction of $E(B - V) = 0.17$ increases the allowed fading to 3–4 mag in most cases and to $\geq$6 mag in the bluest three CNELGs.[9] Extending the amount of fading time to the look-back time for the highest redshift of the sample allows ~4 mag of fading, and decreasing it to the lowest redshift decreases the allowed fading to ~3 mag. Reducing the assumed metallicity to 0.02 $Z_\odot$, which may be appropriate for the smallest dwarfs but is not warranted by the small amount of existing data for CNELGs (Kobulnicky & Zaritsky 1999), decreases the fading allowed in 5 Gyr to ~2.5 mag.

[8] We use $t_{\rm dyn}(R_e) = 1.014 R_e/\sigma$, which comes from adopting $t_{\rm dyn}(r) = (\pi/2)[GM(r)/r^3]^{-1/2}$ (Binney & Tremaine 1987), and the dynamical mass formula $M = 3(k/G)R_e\sigma^2$ (Guzmán et al. 1996) assuming $k = 1.6$. The values of R_e and σ are from Koo et al. (1994, 1995) and Guzmán et al. (1996).

[9] As noted in Table 1, the three bluest CNELGs are not necessarily the smallest. One is consistent with the size of NGC 205, but two out of three are consistent only with the much larger VCC 437.

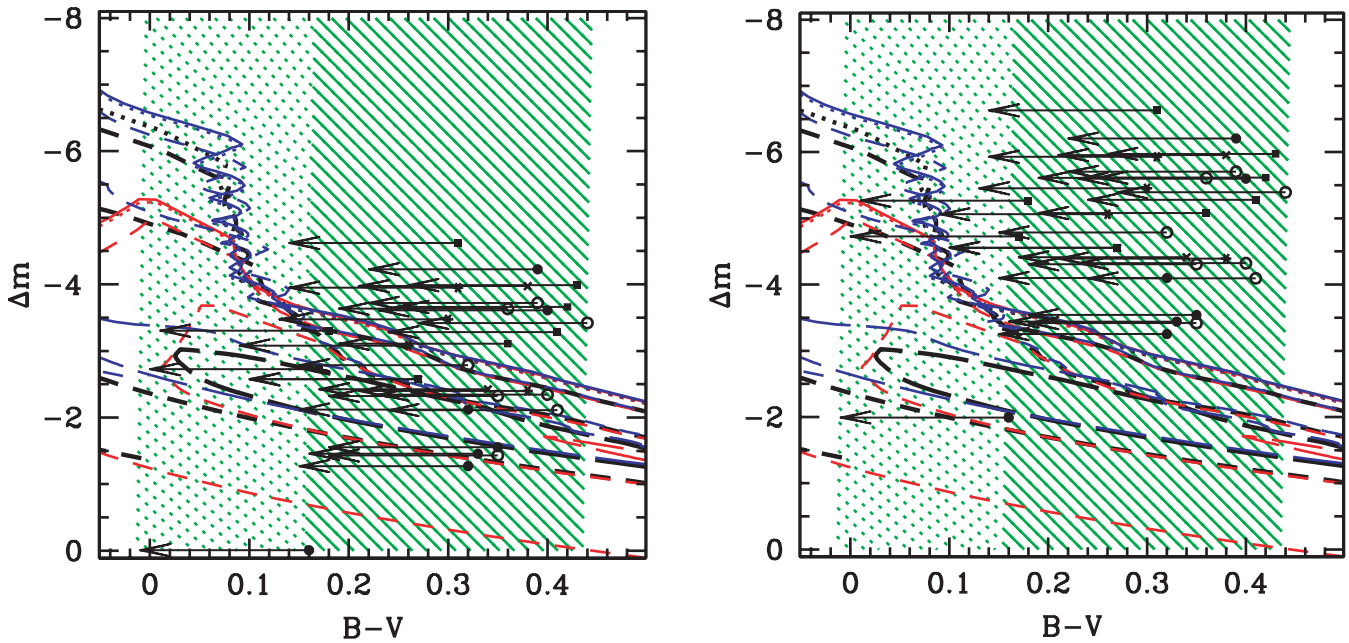

FIG. 7.—Rest-frame color as a function of number of magnitudes the burst will fade by the time 5 Gyr has elapsed since the burst. The lines are the models as in Fig. 6. The symbols show the CNELGs that are NGC 205–like (*filled circles*), intermediate between NGC 205 and VCC 437 (*open circles*), VCC 437–like (*filled squares*), and large (*asterisks*), as well as the additional luminous compact blue galaxies (*crosses*). We plot each point at its observed rest-frame $B - V$ color on the x-axis vs. the number of magnitudes the CNELG needs to fade to become the brightest dwarf in the van Zee sample, VCC 1261, with $M_B = -17.4$ (*left*), or the number of magnitudes the CNELG needs to fade to become the faintest dwarf in the van Zee sample, VCC 1743, with $M_B = -15.2$ (*right*). The arrows indicate the rest-frame $B - V$ colors assuming a reddening of $E(B - V) = 0.17$.

Despite the effects of burst duration on the peak luminosity boost allowed by a given burst of star formation, the relationship between the total amount a starburst can fade and the color of the galaxy is nearly independent of the timescale of the burst. In Figure 7 we plot this relationship for the models shown in Figure 6. The figures show rest-frame color as a function of number of magnitudes the burst will fade by the time 5 Gyr has elapsed since burst. The symbols show the CNELGs and the additional luminous compact blue galaxies. We plot each point at its observed rest-frame $B - V$ color on the x-axis and at the number of magnitudes the CNELG needs to fade to become the brightest dwarf in the van Zee sample, VCC 1261, with $M_B = -17.4$ (*left*), and the number of magnitudes the CNELG needs to fade to become the faintest dwarf in the van Zee sample, VCC 1743, with $M_B = -15.2$ (*right*). Arrows indicate the intrinsic rest-frame $B - V$ if $E(B - V) = 0.17$.

We list the true upper limit to the amount of fading allowed by this analysis in Table 1 calculated using the look-back time to each object (set to 5 Gyr in Fig. 7), both with and without reddening. The upper limits correspond to the position on the solid line for the color of the galaxy in Figure 7 if the models were shifted each time to normalize at the look-back time of the redshift of the CNELG. For example, renormalizing the fading dwarf to correspond to a fading time of 6.43 Gyr, the look-back time at the highest redshift in our sample ($z = 0.728$), instead of the 5 Gyr used in Figure 7, increases the allowed amount of fading by 0.24 mag. In the left and right panels of Figure 8 we plot the minimum faded (present-day) magnitude of each CNELG as a function of redshift with and without the reddening correction, respectively. In any scenario, all of the galaxies can fade to become sub-L^* galaxies with $M_B < -19$. Without the reddening correction and neglecting errors, 14/27 cannot fade to $M_B > -17.4$ (the most luminous dwarf in the van Zee sample) and 26 cannot fade to $M_B > -15.2$ (the faintest in the van Zee sample). With the reddening correction and neglecting errors, seven cannot fade to $M_B > -17.4$ and 24 cannot fade to $M_B > -15.2$. With the reddening correction and the bluest color allowed by the estimated error, all but one of the galaxies can fade to $M_B > -17.4$ and 15 cannot fade to $M_B > -15.2$.

The amount of possible fading we compute from the measured colors and redshifts is not strongly correlated with our classification of the surface brightness profiles of the CNELGs. However, in § 2.1 we estimate that one to three of the CNELGs in our study are actually superposed on flux from background or foreground galaxies. Because these low surface brightness features would not be evident in the spectra of CNELGs, we cannot rule out the possibility that some of the apparently larger CNELGs are actually superpositions. However, the superposed galaxies are not likely to affect the measured colors and the fading analysis. The two luminous galaxies that are roughly as compact as tiny NGC 205 but that cannot fade to even $M_B = -17$ are surprising. However, both galaxies are at relatively high redshifts, where our size analysis has less discriminatory power; as a result, both are also formally consistent with intermediate-sized dwarf galaxies.

From this analysis, we conclude that most CNELGs (96%) could conceivably fade to become at least as faint as luminous dwarf galaxies $M_B > -17.4$, although it is by no means guaranteed that they will fade to these limits. We predict that at most 11% of CNELGs fade to become very low luminosity dwarf galaxies ($M_B > -15.2$).[10] The remaining CNELGs fade by smaller amounts to the present epoch, to become sub-L^* galaxies or luminous dwarfs. Thus, the "bursting faint dwarf" model works for *at most* 11%–44% of CNELGs. The others must fade to become higher luminosity dwarfs or more luminous galaxies. In

[10] Accounting for the estimated errors in $B - V$, this analysis shows that less than 44% can fade to this limit given the bluest possible colors consistent with the data.

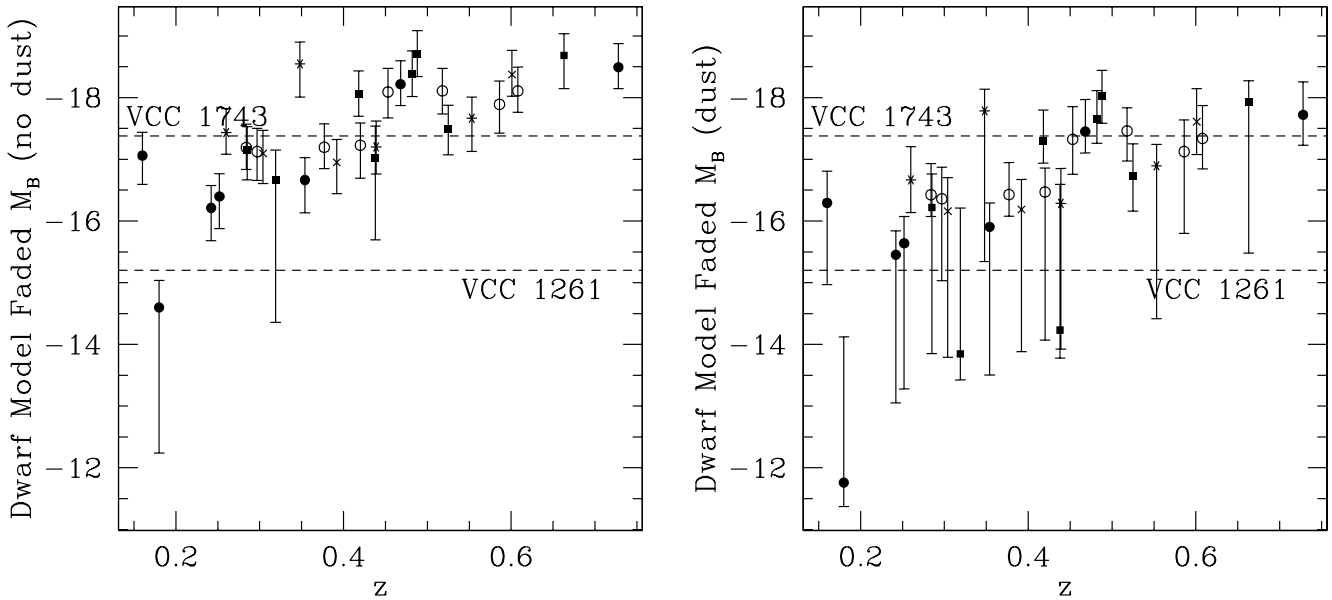

FIG. 8.—Maximum present-day magnitudes (or minimum present-day luminosities) of the CNELGs as a function of measured redshift, computed from the maximum amount of fading allowed by the color and look-back time for solar metallicity assuming no reddening (*left*) or $E(B-V) = 0.17$ (*right*). Error bars reflect an error in rest-frame color, $(B-V)_0$, of 0.1 mag. Symbols are as in Fig. 7. The horizontal dashed lines indicate the luminosity range of the Virgo dE sample of van Zee et al. (2004a).

§§ 3.2–3.4 we explore alternative scenarios that involve more massive galaxy descendants.

3.2. *The Bulges-in-Formation Hypothesis*

The analysis of § 3.1 demonstrates that the bursting dwarf hypothesis is not a satisfactory explanation for all of the CNELGs because some CNELGs are too large to fade to dEs and some are not likely to fade enough. In §§ 3.2–3.4 we explore the alternative possibility that some CNELGs are actually starbursts in the centers of intrinsically more massive galaxies that fade by $\lesssim 2$ mag to become present-day luminous galaxies (Koo et al. 1995; Kobulnicky & Zaritsky 1999).

Here we explore the possibility that CNELGs are bursts of star formation in the centers of spiral galaxies. If these starbursts form a substantial population of new stars in the centers of the galaxies, they are almost certainly associated with the in situ formation or enhancement of a galactic bulge. In this scenario, the narrow kinematic emission line widths of the CNELGs may result from the fact that the starburst is centrally concentrated. The emission-line flux samples only the central part of the galaxy's potential well (Kobulnicky & Gebhardt 2000; Barton & van Zee 2001; Pisano et al. 2001). Similarly, CNELGs may be central starbursts in disks viewed face-on (Homeier & Gallagher 1999; Homeier et al. 2002).

Bulges in formation may be very difficult to discern. The low mass-to-light ratio of even a small forming bulge allows it to dominate the flux of a spiral galaxy during rapid formation (e.g., Fig. 3 of Barton & van Zee 2001). In this scenario, the galaxy as a whole fades less to the present epoch, but its surface brightness distribution changes dramatically. When the forming bulge fades, the disk becomes much more obvious and the object appears as a disk galaxy instead of a CNELG.

Because CNELGs are selected as compact objects, they are not embedded in extremely obvious galactic disks. With the exception of 212668, which has an evident tidal tail in the new data, our deep ground-based data do not reveal incontrovertible evidence for disks based on visual inspection alone. However, lower surface brightness disks and small disks would not be evident in a visual inspection. The analysis in § 3.1 demonstrates that only four of the CNELGs, those in the "LARGE" category (that includes 212668), are more extended spatially than even large dwarf galaxies.

As Figure 3 illustrates using the de Jong (1996) local sample of spiral galaxies, most isolated disks at redshifts $\lesssim 1$ would be resolved by our data. However, the inner disks may be overwhelmed by light from the central starburst in some CNELGs. To be observed clearly in a distant galaxy, the disk must exceed the surface brightness limit of the observation at a radius well beyond the influence of the central burst. Thus, our ability to detect a disk depends on both the central surface brightness of the disk and its scale length: larger, higher surface brightness disks are easier to see. The ability to discern a disk is also a strong function of redshift because of cosmological surface brightness dimming; distant disks can fade into the sky noise without extending very far past the influence of the bulge (or central starburst). Finally, disk detection depends on the luminosity of the central starburst, or equivalently the bulge-to-disk ratio, because the luminosity of the central source affects the radius at which its light dominates the disk. For these reasons, we explore the detectability of disks in our CNELGs one at a time using models constructed at the redshift and resolution appropriate for each CNELG.

In the absence of a "smoking gun" for disks, we use our data to explore the possibility that CNELGs are embedded in disks by computing the surface brightnesses of the brightest disks of a given size that could be accommodated by our data. Figures 9 and 10 show the circular surface brightness profiles of two CNELGs plotted on top of circular surface brightness profiles of models of isolated face-on disks with Sbc-type SEDs that were added to blank-sky regions of the data. The plots are similar for moderately inclined disks. Highly inclined disks are likely ruled out because they would be evident in the data, giving the galaxies a "pinched" appearance.

The figures show the sample disks near the maximal limits for a marginally unresolved CNELG (Fig. 9) and a well-resolved, spatially extended CNELG (Fig. 10). Our data rule out disks that fall above the surface brightness of the CNELG at large radii.

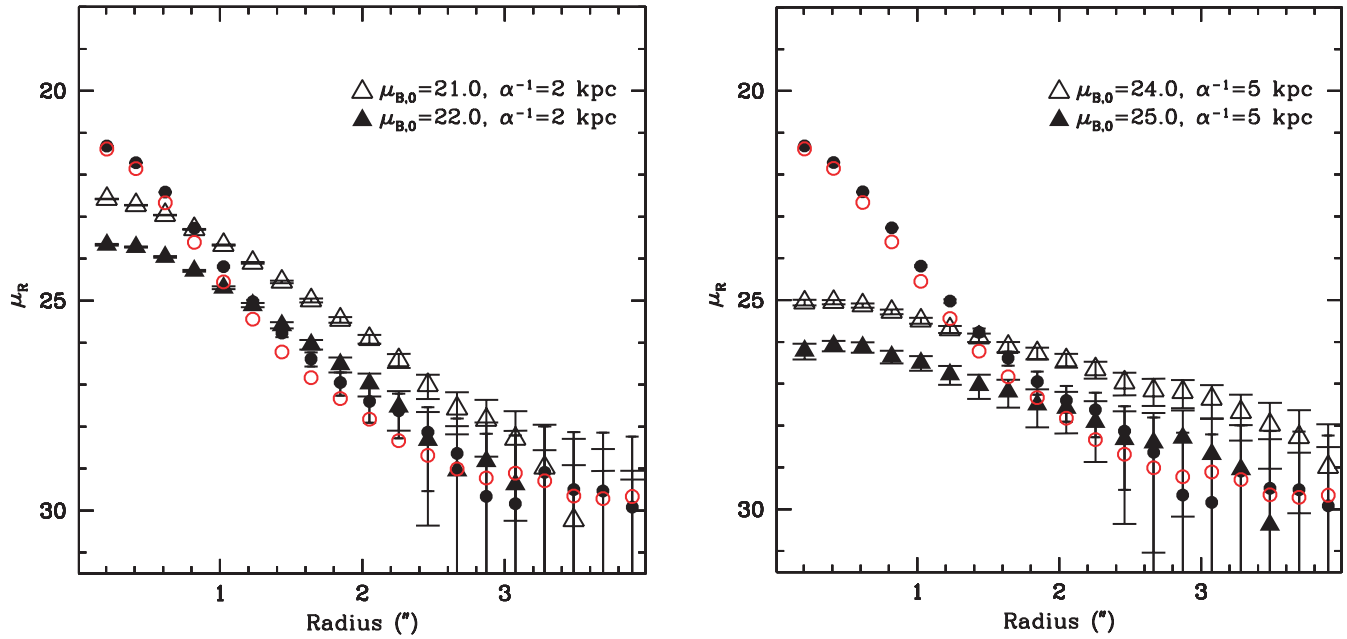

FIG. 9.—Models of pure exponential disks underlying CNELGs. For 217169 at $z = 0.354$, we plot circular surface brightness profiles of the CNELG (*filled circles*) with nearby PSF stars (*open red circles*) and face-on disk models (*filled and open triangles*) added to the same data. Labels in the upper right corner indicate the rest-frame central surface brightnesses and scale lengths of the disk models. We show models for two different disk sizes: a 2 kpc disk (*left*) and a 5 kpc disk (*right*).

The results illustrated by Figure 9 are typical of the NGC 205–like CNELGs in our study (see the classifications in Table 1). These CNELGs are not spatially extended enough to accommodate most of the local disks larger than ~2 kpc in the de Jong (1996) sample. The detailed limits set by this analysis are a strong function of redshift. The lowest redshift NGC 205–like CNELGs can accommodate essentially no realistic face-on disks. CNELG 111255 requires $\mu_{B,0} \gtrsim 24$ for even a 2 kpc disk.

For example, in the left panel of Figure 9 we illustrate that our data could accommodate a 2 kpc disk with $\mu_{B,0} = 22$ (for an Sbc-type SED), but not one with $\mu_{B,0} = 21$. The right panel shows that the data accommodate a 5 kpc disk with $\mu_{B,0} = 25$, but not one with $\mu_{B,0} = 24$. Substantially larger disks (e.g., 10 kpc) with realistic surface brightnesses ($\mu_{B,0} < 24$) are nearly always ruled out. Even Malin 1, with $\mu_{B,0} \sim 25.5$ but $R_d = 78$ kpc (Impey & Bothun 1989), would be quite evident in the data.

As Figure 3 illustrates, the known disks typical in the local universe occupy a limited range of surface brightnesses, although this range may be artificially truncated by selection effects even in the local universe. While there are 2 kpc disks with $\mu_{B,0} > 21$, there are very few 5 kpc disks with $\mu_{B,0} \gtrsim 24$. Thus, we conclude from Figure 9 that if the nearly unresolved CNELG 217169 is embedded in a disk, it is either much lower surface brightness than most known disks in the local universe or quite small (~2 kpc).

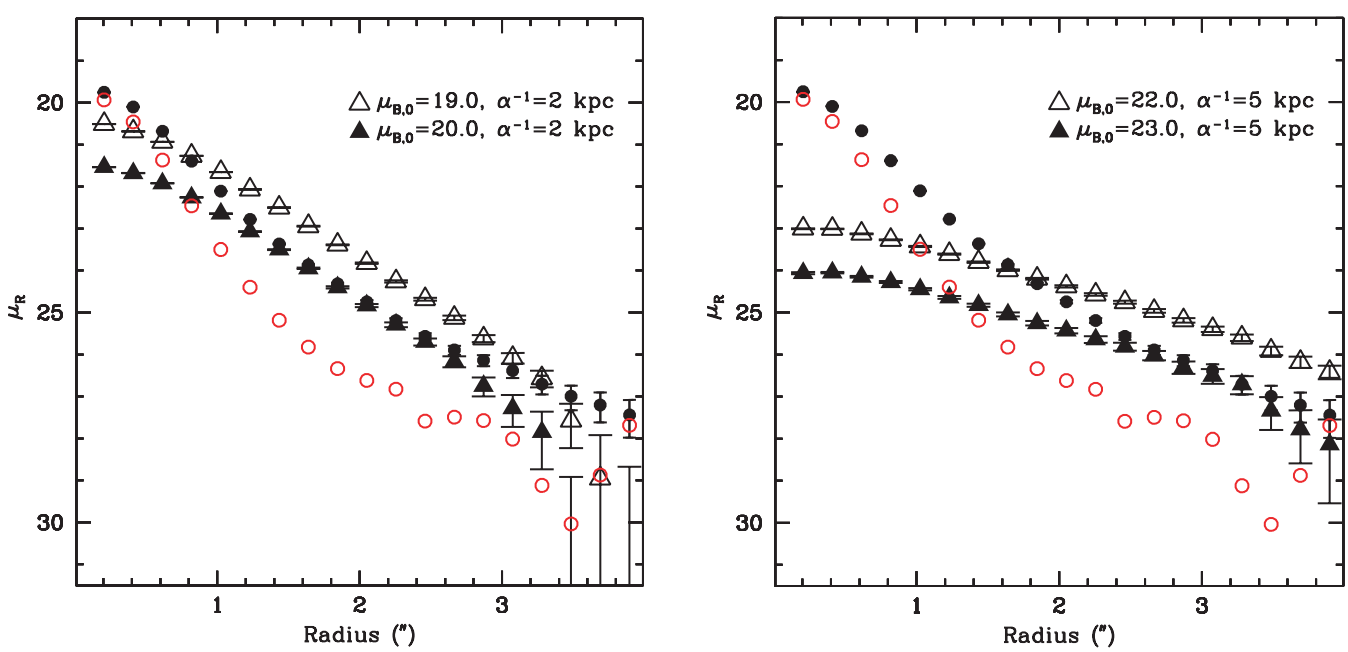

FIG. 10.—Models of pure exponential disks, with symbols as in Fig. 9, but for different model parameters and for the LARGE galaxy 217255 at $z = 0.348$.

TABLE 2
MAXIMAL $\mu_{B,0}$ FOR FIXED-SIZE DISKS

Field (1)	ID (2)	$\mu_{B,0,\max}$ 2 kpc Disk (3)	5 kpc Disk (4)	10 kpc Disk (5)
SA 57O	111867	23.3	25.7	26.6
SA 57N	111255	24.1	26.2	>27.0
SA 68E	208846	23.1	25.4	26.5
SA 57P	112259	22.8	26.0	>27.0
SA 68F	212668	21.5	23.7	25.2
SA 68H	217054	21.9	24.5	25.9
SA 68C	206134	21.5	24.5	25.9
SA 68A	203307	22.0	24.4	25.6
SA 57K	108954	21.1	23.9	25.3
SA 68J	217255	19.9	22.7	24.2
SA 68I	217169	22.0	24.3	25.6
SA 68L	217779	21.4	24.0	25.7
SA 68G	212916	20.4	23.2	24.8
SA 57Q	112536	21.3	23.6	24.9
SA 57G	110601	20.2	23.0	24.7
SA 57L	108956	21.0	23.4	24.7
SA 57D	105482	20.2	22.8	24.3
SA 68D	206403	20.2	23.2	24.8
SA 68N	215428	20.1	23.4	25.3
SA 68O	216388	19.9	22.8	24.6
SA 57R	117671	20.3	23.0	24.5
SA 57F	107042	20.8	23.1	24.7
SA 68K	217418	20.2	22.4	23.9
SA 57S	118170	19.7	22.3	24.0
SA 57J	108945	19.7	22.7	24.4
SA 57H	117731	19.1	21.5	22.9
SA 68M	209640	19.2	22.0	23.6
Compact Galaxies				
SA 68B	205935	21.2	23.8	25.3
SA 57B	103605	20.7	23.6	25.0
SA 57C	104259	19.3	22.0	23.6

NOTES.—The maximal central surface brightness of disks accommodated by our data. Col. (1): Field. Col. (2): ID number. Cols. (3), (4), and (5): Maximal *B*-band surface brightness for a disk with an Sbc-type SED and a scale length of 2, 5, and 10 kpc, respectively. We note that maximal central surface brightnesses become substantially less accurate at $\mu \sim 27$ for 5 kpc disks and at $\mu \sim 25$ for 10 kpc disks.

We compute the approximate maximum disk surface brightness accommodated by the CNELGs. We compare model disks (with noise) to the CNELGs in the outer radii beginning where the model disk flux first exceeds the CNELG flux. We create models at 1 mag intervals in central surface brightness and interpolate to the disk surface brightness that corresponds to $\chi^2/\mathrm{dof} = 1$ in these outskirts. We list the results for Sbc-type disks in Table 2, sorted by redshift. For two cases, we quote only a lower limit to the maximum surface brightness (i.e., if 112259 has a 10 kpc disk, its central surface brightness is $\mu_{B,0} \gtrsim 27$). Assuming that the disks have bluer (Im-type) SEDs changes the *B*-band surface brightnesses by $\leq$0.3 mag. For context, we know that the fiducial "Freeman" (bright) disk has a central surface brightness of $\mu_B = 21.65$ (Freeman 1970).

Both 111867 and 208846 accommodate 2 kpc disks with Sbc SEDs only if $\mu_{B,0} \gtrsim 23$; 111255 requires $\mu_{B,0} \gtrsim 24.1$ for a 2 kpc disk and $\mu_{B,0} \gtrsim 26.2$ for a 5 kpc disk. CNELG 112259 requires $\mu_{B,0} \geq 22.8$ for a 2 kpc disk and $\geq$26 for a 5 kpc disk, and 217169 (Fig. 9) requires $\mu_{B,0} \gtrsim 22$ for a 2 kpc disk and $\mu_{B,0} \gtrsim 24.3$ for a 5 kpc disk. These five objects are the most unusual in nature. All have $z < 0.4$ and $M_B \gtrsim -20$. We discuss their nature further below. The higher redshift NGC 205–like CNELGs accommodate more common small or low surface brightness disks, as Table 2 indicates.

3.2.1. *Implications of the Maximum Allowable Disks*

The bulges-in-formation picture arose as a solution to the problem suggested by the apparently high metallicities of the CNELGs that have measured abundances. Kobulnicky & Zaritsky (1999) study the gas-phase metallicities of a set of two CNELGs, finding that they lie along the luminosity-metallicity relation of field galaxies. Although we note that there are many exceptions to the luminosity-metallicity relation, such as NGC 205, the naive interpretation of their results may restrict the amount of fading possible to these galaxies: the two CNELGs in the Kobulnicky & Zaritsky (1999) study appear to be too metal-rich to fade to the observed low-luminosity ($M_B \gtrsim -16$) dEs in the local universe. They predict fading for CNELGs that is $\lesssim$1–2 mag. The authors propose that CNELGs are either progenitors to the more luminous and metal-enriched dEs or bulges forming before their disks are evident. However, these detailed metallicities have only been measured for a small number of CNELGs. In addition, the starbursts in CNELGs may represent a relatively small fraction of the total gas at a later stage in the galaxy's history, arguing that the metallicity in the gas phase may be higher than the metallicity of the galaxy as a whole.

Although the present deep imaging data do not prove that most CNELGs are embedded in galactic disks, we explore how the presence of a disk could affect the fading of the CNELGs to the present day. Here we hypothesize that the CNELGs are starbursts in the middle of face-on disks that have the approximate maximum disk luminosities allowed by the surface brightness profiles of the CNELGs (Table 2). Assuming that the objects harbor Sbc-type disks with the maximum allowed central surface brightnesses, most of the 27 CNELGs are "bulge-dominated" (or starburst-dominated) objects, with $\langle B/T \rangle = 0.6$ for the 2 kpc disks and $\langle B/T \rangle = 0.8$ for the 5 kpc disks. For these maximum allowable disks, these numbers are lower limits to the average B/T (or starburst/T) ratios of the CNELGs.

If the disks do not evolve in luminosity or size but the central starbursts fade substantially, the B/T ratios of the objects decline rapidly (see, e.g., Barton & van Zee 2001). At the same time, the total luminosities of the galaxies evolve, but by much less than the fading central starbursts evolve. In this way, the luminosity in the disk "stabilizes" the CNELG against fading. Here we assume SEDs for the disks and that the disks do not evolve substantially in luminosity or color, then explore the fading caused by fading of the "bulge" component in two ways, by considering (1) the amount of fading allowed to bring the galaxy's B/T ratio to a given final value and (2) the amount of fading that will occur by the present day assuming that the color of the observed CNELG must match the color of the composite "bulge"+disk at the redshift of the CNELG.

Fading to a given B/T ratio.—In Figure 11 we explore the amount of total object fading that results from the fading of the bulge to an eventual bulge-to-disk ratio that is more typical of spiral galaxies. We assume the maximum compatible disks described above. Thus, we show an approximate lower limit to the amount of total object fading required to achieve a $B/T = 0.06$ for the faded object, which is appropriate for the progenitor of a typical small late-type spiral (see, e.g., de Jong 1996). The objects would require less fading to achieve larger B/T ratios appropriate for an earlier type spiral. We plot the required fading to $B/T = 0.06$ as a function of redshift to illustrate the mild systematic trends with redshift that result from the heterogeneity of the sample and our decreasing ability to rule out more luminous disks at

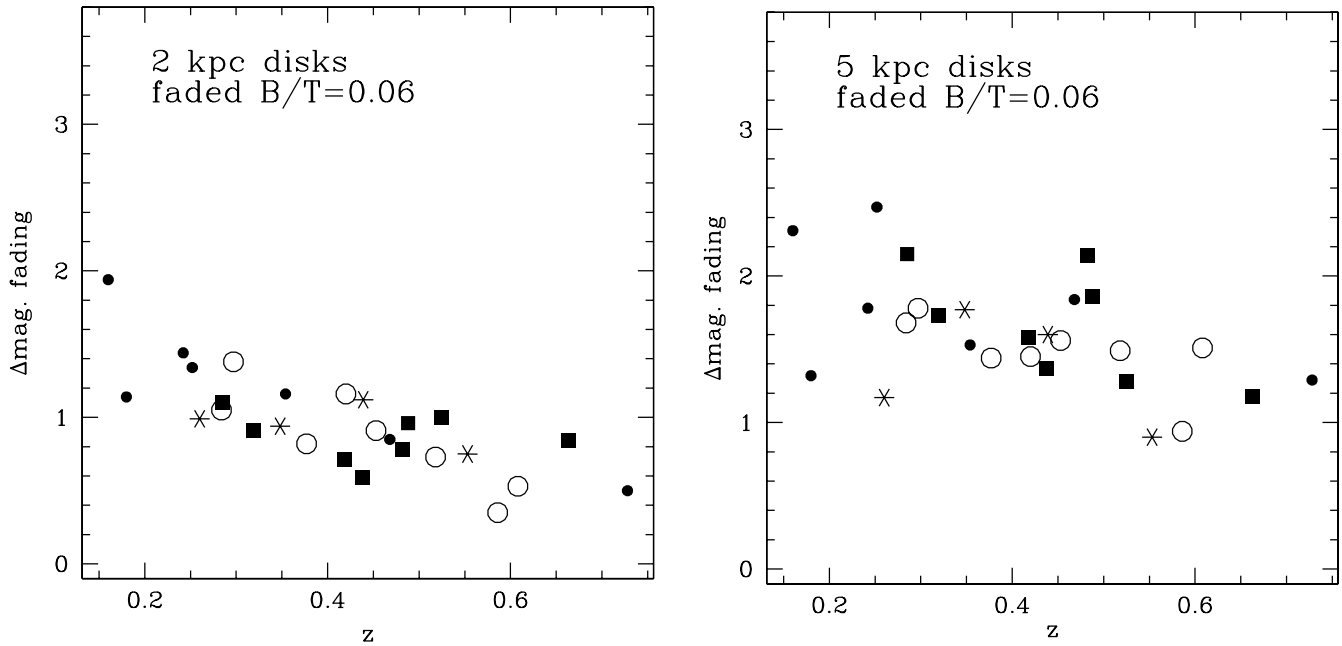

FIG. 11.—Assuming the maximum allowable (face-on) disk described in § 3.2 and a nonevolving disk luminosity, we plot the amount of total object fading required to achieve a $B/T = 0.06$ for a 2 kpc disk (*left*) or a 5 kpc disk (*right*) when the bulge is done fading. We show NGC 205–like (*filled circles*), INTERMED (*open circles*), VCC 437–like (*filled squares*), and LARGE (disklike) CNELGs (*asterisks*).

higher redshifts. The classes of CNELGs from Table 1 are differentiated by point styles.

The relationship between $B - V$ color and amount of fading defined by the models in Figure 6 allows us to examine whether this picture is consistent with the colors of CNELGs. In some cases, the objects are too blue to support this picture: even if the disk is blue (Im type) and remains stable in color and B-band luminosity, the bulges must fade to $B/T < 0.06$ to explain the color of the composite CNELG.

Color matching.—If we fix the color of the disk and match the color of the composite object to the color of the actual CNELG, allowing any final ratio $B/T \geq 0$, the objects themselves fade by less than 2 mag to match their colors if they are surrounded by Sbc-type ($B - V = 0.58$), Scd-type ($B - V = 0.5$), or Im-type ($B - V = 0.34$) disks of maximal surface brightness. We note that some of these disk colors are not blue enough to allow a color equal to the object color for a final, faded $B/T \geq 0$; in these cases we only allow the bulge to fade to $B/T = 0$. Figure 12 shows the faded magnitudes of the CNELGs in this model. With the maximum allowed disk, the objects fade little and most remain luminous; 89% (24/27) have mean faded $M_B \leq -17.4$. Conversely, the four low-redshift objects whose maximal fading is below $M_B = -18$, 111867, 111255, 208846, and 112259, almost certainly cannot be luminous galaxies. Even without fading they have $M_B > -19$. These are among the five objects identified in § 3.1 as the best candidates for starbursting dwarf galaxies. The fifth, 217169, has a faded mean $M_B = -18.1$. Because of the "stabilizing" disk population, reddening can have little effect on Figure 12. Assuming $B - V$ colors that are 0.3 mag bluer changes the mean results by an average of only 0.14 mag for the 27 CNELGs. If the disks increase in luminosity through continued star formation, the objects fade by even less than the predicted amount. Conversely, if the disks fade, the objects will fade, but this effect is very general and equally applicable to discussions of all disk galaxies at intermediate redshift.

If most CNELGs actually harbor disks, they will fade by roughly ~1–2 mag and most will remain luminous galaxies ($M_B \lesssim -18$). As Figure 12 illustrates, the maximum allowable small disks support enough stellar mass to stabilize most of the galaxies against fading to dwarfs. Only 4/27 CNELGs essentially must fade to $M_B \gtrsim -18$.

3.3. *The Cores of Elliptical Galaxies in Formation*

The surface brightness profiles of most of the nearby CNELGs in our study rule out the existence of a red underlying population with the structural parameters of a giant elliptical. However, the redshift dependence in our ability to detect an underlying older

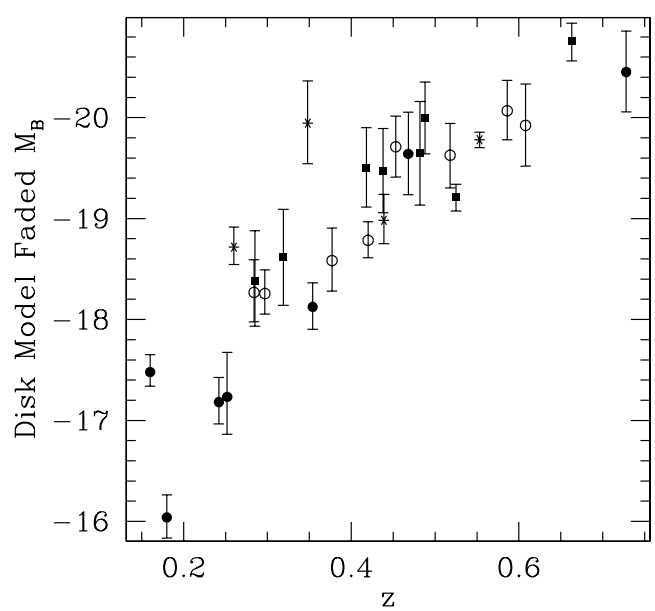

FIG. 12.—Present-day luminosities of the CNELGs if they fade according to the model in § 3.2.1 based on maximizing the surface brightness of potential "hidden disks" in which they are embedded. The spread indicated by the error bars corresponds to the range of results for different disk SEDs and for the 2 kpc disk and 5 kpc disk models. Symbols are as in Fig. 7.

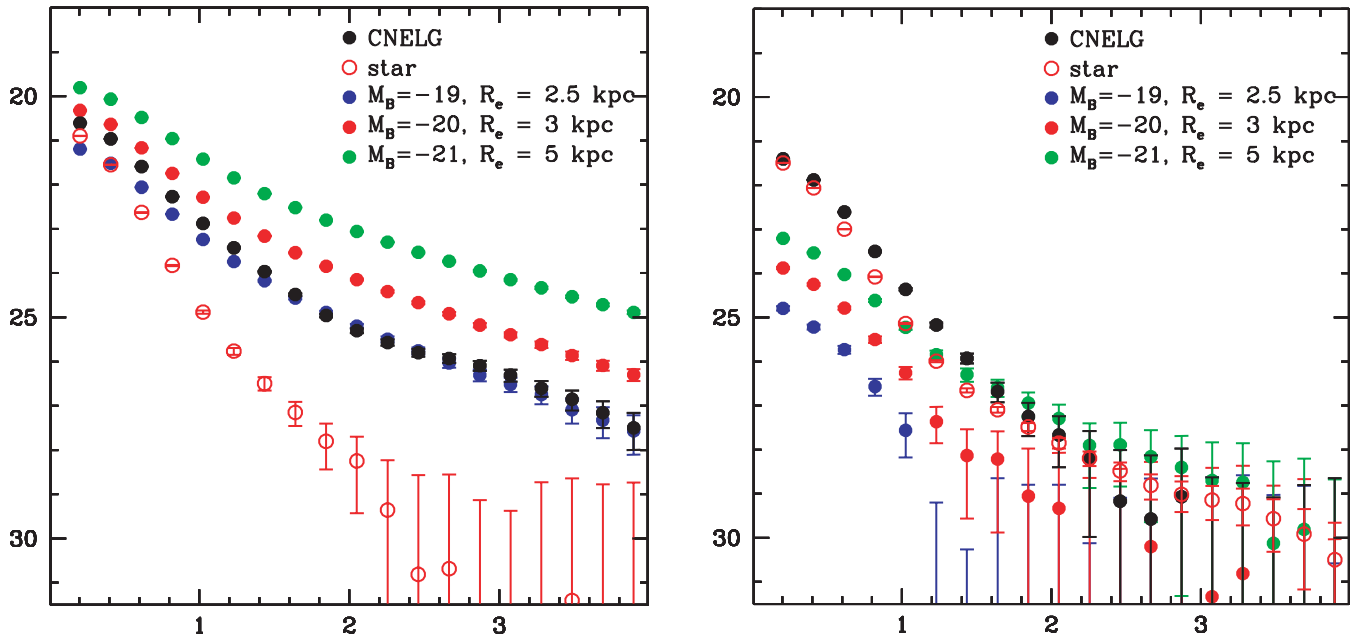

FIG. 13.—Models of $R^{1/4}$ law elliptical galaxies underlying CNELGs. For 212668 at $z = 0.260$ (*left*) and 209640 at $z = 0.728$ (*right*), we plot circular surface brightness profiles of the CNELGs (*filled black circles*) with nearby PSF stars (*open red circles*) and elliptical galaxy models (*blue, red, and green filled circles*) added to the same data. Labels in the upper right indicate the rest-frame luminosities and effective radii of the elliptical galaxy models.

galaxy is extremely strong because of the much larger *k*-corrections associated with older stellar populations. In Figure 13 we show the surface brightness profiles of model elliptical galaxies on the profiles for two CNELGs, 212668 (*left*), which is actually a LARGE galaxy at lower redshift, and 209640 (*right*), an NGC 205–like galaxy at the highest redshift of the sample, $z = 0.728$. We are unable to rule out giant elliptical galaxies from the surface brightness profile of the distant galaxy, even though it is very compact. However, very luminous elliptical galaxies are ruled out for the LARGE galaxy. In this example, our ability to find underlying red stellar populations is dominated by redshift and not by the actual measured extent of the galaxy. Because of this extremely strong redshift dependence, the surface brightness profile provides little useful information about the presence of a very old stellar population.

The strongest arguments against the hypothesis that CNELGs and other compact blue galaxies at intermediate redshift are giant elliptical galaxies involve kinematics (e.g., Im et al. 2001). The velocity widths of CNELG emission lines are narrower than the absorption-line widths of nearly all elliptical galaxies. Concentrating the star formation in the center of an elliptical to form a CNELG is unlikely to solve the line width problem because many elliptical galaxies have velocity dispersions that rise in the center (e.g., Franx et al. 1989; Im et al. 2001). Some elliptical galaxies have a distinct central component organized into a disk. If the disk formed rapidly with a central burst of star formation in the elliptical, the system might resemble a CNELG for a brief time. However, the nearby disks in elliptical galaxies observed at high spatial resolution appear to have similar star formation histories to their parent galaxies (Carollo et al. 1997). Lower luminosity elliptical galaxies provide another possibility, but the majority of even these low-mass systems also have larger velocity dispersions than the CNELGs (e.g., Halliday et al. 2001).

3.4. *CNELGs as Progenitors of E+A Galaxies*

By definition, E+A galaxies have strong Balmer absorption lines and little or no line emission. Thus, they are composed of a mix of older stars and a dominant population of A-type stars, but no younger, more massive stars; their spectra are consistent with a strong burst of star formation that abruptly ceased ~1 Gyr ago (Couch & Sharples 1987; Newberry et al. 1990; Schweizer 1996; González Delgado et al. 1999; González Delgado & Leitherer 1999). Although they are currently only a small fraction of the luminous galaxy population (~0.2%; Zabludoff et al. 1996), they represent a distinct phase of post–strong starburst evolution (Dressler & Gunn 1983; Zabludoff et al. 1996; Quintero et al. 2004). Long-slit spectroscopy demonstrates that the young components of the stellar populations of E+A galaxies are more centrally concentrated than the older stars (Norton et al. 2001). Although detailed morphologies of the separate young and old populations are not available, morphological studies with *HST* of a subset of E+A galaxies reveal disturbed galaxies dominated by spheroids with small half-light radii; at least some of the tidal features are low surface brightness and thus too difficult to see at intermediate redshifts (Yang et al. 2004). Thus, it is quite possible that many, if not all, E+A galaxies are descendants of CNELGs. Because the definition of an E+A is independent of morphology, this hypothesis and those outlined in §§ 3.2 and 3.3 are not mutually exclusive. To put it another way, with a sufficiently strong and short burst (e.g., akin to the bursting dwarf scenario), CNELGs must go through an E+A phase.

High-resolution images of a subset of five extremely blue noncluster E+A galaxies show that they are spheroid dominated ($B/T > 0.5$), although two out of five E+A galaxies with published *HST* images have spiral disks (Yang et al. 2004). Because kinematic studies of E+A galaxies reveal little rotation, Norton et al. (2001) argue that E+A galaxies likely evolve into dynamically hot, spheroid-dominated systems. Thus, the CNELGs that are progenitors to E+A galaxies probably evolve into elliptical galaxies or early-type spiral galaxies. Indeed, Bershady et al. (2005) find that six out of seven CNELGs with *HST* Space Telescope Imaging Spectrograph (STIS) long-slit spectroscopy have $V/\sigma < 1$, i.e., in the spheroidal range.

Similar to the problems posed by identifying CNELGs with elliptical galaxies (§ 3.3), the kinematics of the CNELGs continues to represent a barrier to identifying them with E+A galaxies. Norton et al. (2001) measure a range of velocity widths, σ, for the old stellar populations of E+A galaxies that place them only 0.6 mag brighter than the Faber-Jackson relation (Faber & Jackson 1976). The measured values of σ vary from $\lesssim 23$ to 241 km s^{-1}. Furthermore, the values of σ measured from absorption lines associated with the young stellar populations are on average larger than those for the older populations. The differences may result from systematic differences between the kinematics of a young emission-line population and its kinematics in absorption after $\sim$1 Gyr of aging. However, Kobulnicky & Gebhardt (2000) find no evidence for systematic differences between emission-line widths and absorption-line widths in a sample of 22 local galaxies that span a wide range of morphologies. Alternatively, perhaps the only E+A galaxies that go through CNELG phase are those with the narrowest line widths, which is possible if the E+A galaxies with the narrowest line widths are also the most compact. Existing studies of E+A galaxies are not large enough to uncover a trend of this sort.

4. DISCUSSION AND IMPLICATIONS

The two basic pictures for CNELG evolution can be categorized as (1) the bursting dwarf hypothesis, where the galaxies are intrinsically low-mass systems that fade to become present-day dwarfs, and (2) the hypothesis that CNELGs are the centers of more massive galaxies that fade little and remain luminous to the present day ($L \gtrsim 0.1L^*$). In §§ 3.2 and 3.3 we discuss variants on the latter hypothesis: (1) that CNELGs are starbursts in the centers of disk galaxies, possibly related to the formation of galactic bulges (§ 3.2), (2) that CNELGs are cores in elliptical galaxies (§ 3.3), and (3) that CNELGs are the immediate progenitors of E+A galaxies (§ 3.4). Hypothesis 2 is very general and may include many different types of formation scenarios.

To explore the dwarf model, we calculate the maximal amount of fading to the present day allowed by the look-back times and colors of the CNELGs. To explore the hypothesis that CNELGs are the centers of more massive galaxies, we consider a scenario in which the CNELG is surrounded by the largest exponential older (Im to Sbc-like) stellar population accommodated by its surface brightness profile. We assume that the disk does not fade or change color with time and find the amount of fading that matches the color. Because the surrounding older stellar population stabilizes the galaxy against fading, this technique essentially allows us to compute a minimal amount of fading in the case of a nonevolving disk. If the disk increases in luminosity with time, however, the object will fade less.

The surface brightness profiles we measure indicate that if CNELGs are embedded in disks, most of them are embedded in low surface brightness disks. We note, however, that this hypothesis is broadly consistent with at least one favored formation scenario for the bulge of the Milky Way. The bulge probably formed from a rapid burst of star formation at early times (e.g., Ferreras et al. 2003). Although the disk has a high surface brightness now, it has formed stars and increased in surface brightness from much earlier times to the present epoch. Thus, at the time the bulge formed, the disk may have been below the central surface brightness limits allowed by Table 2. Although the Milky Way bulge almost certainly formed long before $z = 0.728$, the basic formation scenario indicates that the Milky Way may have gone through a CNELG-type phase if its disk was low surface brightness when its bulge formed.

4.1. *Sorting Different Types of CNELGs*

Both the literature and our analyses support the conclusion that CNELGs are a heterogeneous class of objects. The CNELG sources studied here were selected with three main attributes: (1) they are unresolved sources in moderate-seeing ground-based images, (2) they are selected from a magnitude-limited sample, and (3) they are selected to have blue colors unlike Galactic stars. The apparent magnitude–limited nature of the sample results in a strong correlation of luminosity with redshift. Roughly, sources above $z = 0.4$ are brighter than $M_B = -20$, while lower redshift sources are fainter than $M_B = -20$. Surface brightness limits on embedded disks (§ 3.2) are similarly correlated with redshift, with $\mu_{B,0,\max} = 21$ mag arcsec^{-2} corresponding to the break point at $z = 0.4$. On the other hand, because the color selection was narrowly defined and k-corrections for these blue colors are small, there is little to no trend in rest-frame color with redshift. As Figure 4 illustrates, even at the highest redshift in our sample we can distinguish a small dwarf like NGC 205 from a large dwarf like VCC 437. We can also distinguish both types from much larger galaxies. Most surprisingly, however, the size classes based on the analysis in this paper are also not strongly correlated with redshift, with the exception of the extreme compactness of the four lowest redshift CNELGs. With these considerations of homogeneity and heterogeneity in mind, we can combine constraints gleaned from the CFHT imaging presented here with other information to gain insight into their nature.

We summarize the two basic models of dwarf galaxies from §§ 3.1 and 3.2 in Figure 14. On the left, the colored histograms correspond to the dwarfs of different sizes for the maximal fading model. On the right, the colored histograms correspond to the "maximal" disks of 2, 5, and 10 kpc accommodated by the surface brightness profiles of the CNELGs (Table 2).

For the "starbursting dwarfs" model that assumes that CNELGs will fade maximally, the left panel of Figure 14 shows histograms of the LARGE, VCC 437–like, INTERMED, and NGC 205–like classes of CNELGs (*top to bottom*). All but the LARGE class of dwarfs overlap dEs in the local universe. However, for many of the most luminous CNELGs, the required faded central μ_B is brighter than typical dwarfs in the local universe, especially if we assume no reddening correction (*cyan histograms*). These objects either (1) are all reddened, (2) do not fade as much as the maximal model suggests, or (3) fade to small galaxies that are more luminous than the dwarf population that is typically studied today. The LARGE class of galaxies overlaps only with the lower surface brightness small disks in this maximally fading model.

For the "hidden disks" model that assumes that CNELGs will fade minimally, stabilized by an older population in a surrounding disk, the right panel of Figure 14 shows histograms of the brightest 2, 5, and 10 kpc disks accommodated by the data. All but four CNELGs can harbor 2 kpc disks with parameters that overlap disks in the nearby universe. In contrast, most cannot harbor 5 kpc disks with typical parameters, and almost none can harbor 10 kpc disks. Thus, if CNELGs are starbursting centers embedded in typical galactic disks, their disks are small.

The four lowest redshift objects, 111867, 111255, 208846, and 112259, are classified as NGC 205–like, suggesting that at redshifts below $\sim$0.3 the extremely compact size requirements for the original definition of CNELGs prohibit the selection of extended galaxies. As observed, they are already relatively low luminosity, with $-18.8 \leq M_B \leq -17.2$. Their colors, luminosities, and redshifts suggest that within the errors they can fade to even $M_B \gtrsim -15$ (§ 3.2), and their surface brightness profiles and colors suggest that they must fade to at least $M_B \gtrsim -17.5$.

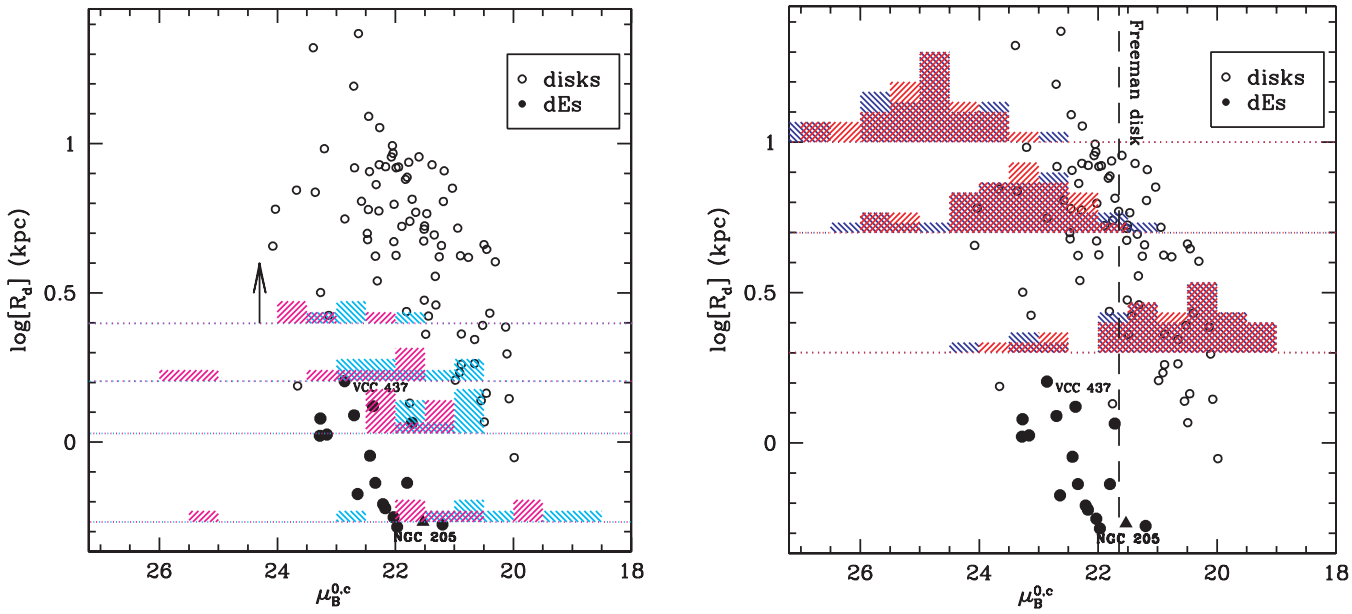

FIG. 14.—Parameters of faded CNELGs in the maximal-fading model of Fig. 8 (*left*; § 3.1) and the minimal-fading model corresponding to Fig. 12 (*right*; § 3.2) shown with parameters for local dwarfs and disks as in Fig. 3. For the maximal-fading model, we assume exponential light profiles and plot histograms of the dwarfs at their resulting central *B*-band surface brightnesses of the faded dwarfs assuming that the NGC 205–like, INTERMED, VCC 437–like, and LARGE dwarfs have sizes of 0.54, 1.07, 1.6, and 2.5 kpc, respectively. The arrow indicates that the assumed size of 2.5 kpc is an approximate lower limit for the LARGE class. The magenta histograms are for fading including the reddening correction, and the cyan histograms assume no reddening. For the minimal-fading model, we plot the most luminous disks accommodated by the outer CNELG surface brightness profiles at 2, 5, and 10 kpc (as in Table 2). The red and blue histograms assume Sbc and Im SEDs, respectively.

Thus, the imaging data and the two models point to the same interpretation: these four galaxies are starbursting dwarfs at low redshift, observed at look-back times of $\lesssim 3$ Gyr.

Beyond $z = 0.255$, the classifications of CNELGs appear more mixed. Figures 8 and 12 show the approximate maximum and minimum present-day luminosities of the CNELGs. To within the errors of the right panel of Figure 8, all but one of the CNELGs can fade to $M_B > -17.4$, and 8/23 CNELGs at $z > 0.255$ can fade to $M_B > -16$; the other 15 cannot. In contrast, according to the disk model in § 3.2 (Fig. 12), the (approximate, mean) maximum final luminosities of all of the galaxies with $z > 0.225$ are brighter than $M_B = -17.4$. Thus, all of the CNELGs with $z > 0.255$ could be more luminous than the Virgo dEs at the present epoch (based on the minimal-fading model). Eight of these galaxies could also fade to $M_B > -15.2$ in the maximal-fading model. The remaining 15 must be more luminous than $M_B = -15.2$ at the present epoch. A comparison of the fading limits derived in this study with those of Guzmán et al. (1998) shows broad consistency with their results.

From a morphological perspective, the more extended (LARGE) CNELGs are the most clear-cut examples of luminous galaxies on the basis of their sizes, including 212668, which has an evident tidal tail in the *R*-band image. Their colors allow a large range of possible fading, however, indicating that three of the four can fade to $M_B > -16$ and that all four must fade to the range $-19.9 < M_B < -18.7$. This LARGE subsample consists of only 4 of the 27 (14%) CNELGs. Moreover, we found in § 2.1 that, on a statistical basis, one to three of the CNELGs in our study may be superposed on diffuse background galaxies.

The overlap between this study and the Kobulnicky & Zaritsky (1999) metallicity study includes only one object, 206134, in the SA 68 field, with $z = 0.285$ and $M_B = -20.5$, which we classify as VCC 437–like based on its surface brightness profile. Its metallicity, $12 + \log(\mathrm{O/H}) = 8.83$, lies directly on the luminosity-metallicity relation for nearby star-forming galaxies. The gas-phase abundance is high relative to the stellar metallicity of some of today's dSph galaxies. However, other low-mass dwarfs such as the nucleated dE NGC 205 do have comparable metallicity, and indeed other spheroidals such as Sagittarius and Fornax lie significantly above the luminosity-metallicity relation. The model in Figure 8 allows a "maximum" fading to a very faint $M_B = -13.7$ within the errors on the color, and the model in Figure 12 yields an "average minimum" fading to $M_B = -18.4$, where star-forming galaxies with its metallicity are quite typical in the local universe (Tremonti et al. 2004).

If many of the CNELGs really are progenitors to nondwarf galaxies, the observations of the kinematics of CNELGs remain the most difficult to explain. Even some of the galaxies that are classified as LARGE compared to dwarf galaxies have very narrow emission line widths. These galaxies consistently exhibit narrow line widths that are observed nearby only in dwarf galaxies or in some very low luminosity elliptical galaxies and bulges. However, several authors demonstrate that emission-line kinematics can be misleading (Kobulnicky & Gebhardt 2000; Barton & van Zee 2001; Pisano et al. 2001) and that optical emission line widths are systematically low relative to 21 cm H I for galaxies with narrow optical emission line widths (Pisano et al. 2001).

As discussed above, the line widths observed in CNELGs are usually too narrow for even lower luminosity elliptical galaxies, even if the emission-line flux is centrally concentrated (Im et al. 2001). However, if the emission-line flux originates from a small central disk, the situation may be somewhat different. Small circumnuclear disks have been observed in both spiral and elliptical galaxies (Rubin et al. 1997; Carollo et al. 1997 and references therein). They are often the sites of rapid star formation and, in spiral galaxies, may be associated with the formation of a pseudobulge (e.g., Kormendy & Kennicutt 2004). These disks

exhibit a range of kinematics, however (Rubin et al. 1997). A lack of observed rotational shear in medium spectral resolution long-slit *HST* STIS spectroscopy for six out of seven CNELGs argues against this picture (Bershady et al. 2005), except in the unlikely event that the disks are truly face-on or the minor axis is consistently aligned with the slit. However, at medium spectral resolutions of 7000–10,000, even nearly face-on disks show rotational shear, e.g., as noted for the starburst NGC 7673 (Homeier & Gallagher 1999) or normal spiral galaxies (Andersen & Bershady 2003). Our understanding of how to interpret kinematical data will likely increase with future spectroscopic observations using high-resolution bidimensional spectroscopy.

5. CONCLUSIONS

The compact narrow emission line galaxies (CNELGs) are an extreme, rapidly evolving population of luminous galaxies observed at intermediate redshift (Koo et al. 1994). Their nature and ultimate role in the evolution of galaxies remain heavily debated. We present deep ground-based *R*-band imaging in good seeing designed to detect low surface brightness features that may indicate that CNELGs are starbursts embedded in more massive systems. We combine the new data with existing color and redshift information to draw our conclusions:

1. We use circular aperture surface photometry to set lower limits to their present-day spatial extents irrespective of luminosity, finding that ~26% are consistent with tiny dwarfs like NGC 205 (or smaller, in some cases), 30% are consistent with intermediate-sized dEs, 30% are consistent with larger dwarfs or smaller disk galaxies, and 15% appear more spatially extended than dwarf galaxies.
2. Given the limits of the data, some CNELGs may harbor extended structures such as galactic disks, although only 212668, with a clear tidal tail, shows definitive evidence for one. Our data indicate that if most CNELGs harbor disks, the disks must be small (less than or approximately a few kiloparsecs in many cases) or relatively low surface brightness.
3. Models indicate that 4/27 (15%), the four lowest redshift CNELGs, cannot harbor enough "hidden" disk material to stabilize them against fading to become dwarf galaxies ($M_B \gtrsim -18$). All of these galaxies are nearby ($z < 0.255$) and as small as NGC 205. They are likely examples of bursting dwarfs.
4. From an analysis of the maximum fading possible to CNELGs based on their colors, we find that 15/27 (56%) are not blue enough to fade to tiny dwarf galaxies ($M_B \geq -15.2$), even accounting for reddening and errors. These galaxies remain intrinsically more luminous to the present day. A total of 8/15 of these objects are classified as NGC 205–like or intermediate-sized dwarfs based on their surface brightness profiles.
5. From the same analysis of the maximum fading possible to CNELGs based on their colors, we find that 26/27 (96%) are blue enough to fade to some type of dwarf galaxy ($M_B \geq -17.4$), accounting for reddening and errors. However, four of these galaxies are too spatially extended to become dwarfs.
6. From an analysis of the maximally bright disks accommodated by the measured surface brightness profiles of CNELGs, all but the four CNELGs can harbor small (~2 kpc) disks consistent with small disks observed in the local universe. Most cannot harbor large disks, however. An analysis of the minimal fading allowed to CNELGs based on the potential disks they may harbor indicates that most CNELGs (85%) may fade by only a small amount to remain luminous ($M_B < -18$) at the present epoch.

We thank David Koo, Richard Kron, Steve Majewski, Jeff Munn, and John Smetanka for providing us with redshifts, photometry, and astrometry for the CNELGs in advance of publication. We thank Romeel Davé and James Bullock for helpful suggestions and insight. We thank John-David Smith for his insight into the process of unraveling galaxy morphologies and for assistance that significantly improved our software and data analysis. We thank Elizabeth Adams and Ian Roederer for assisting in the observations of NGC 205. Support for E. J. B. was provided by the Center for Cosmology at the University of California, Irvine and by NASA through Hubble Fellowship grant HST-HF-01135.01 awarded by the Space Telescope Science Institute, which is operated by the Association of Universities for Research in Astronomy, Inc., for NASA, under contract NAS 5-26555; E. J. B. and L. v. Z. also acknowledge the Herzberg Institute of Astrophysics, which is where this work was begun. L. v. Z. acknowledges partial support from Indiana University and NSF grants AST 03-47929 and AST 05-06054. M. A. B. acknowledges NASA/*HST* AR grant 9917 and NSF grant AST 03-07417 and gratefully acknowledges the hospitality he enjoyed during his stay at the University of Toronto, during which time the work was completed.

REFERENCES

Andersen, D. R., & Bershady, M. A. 2003, ApJ, 599, L79
Barazza, F. D., Binggeli, B., & Jerjen, H. 2003, A&A, 407, 121
Barton, E. J., & van Zee, L. 2001, ApJ, 550, L35
Bershady, M. A., Trevese, D., & Kron, R. G. 1998, ApJ, 496, 103
Bershady, M. A., Vils, M., Hoyos, C., Guzmán, R., & Koo, D. C. 2005, in Starbursts: From 30 Doradus to Lyman Break Galaxies, ed. R. de Grijs & R. M. González Delgado (Dordrecht: Springer), 177
Bertin, E., & Arnouts, S. 1996, A&AS, 117, 393
Binney, J., & Tremaine, S. 1987, Galactic Dynamics (Princeton: Princeton Univ. Press)
Bruzual, G., & Charlot, S. 2003, MNRAS, 344, 1000
Carollo, C. M. 1999, ApJ, 523, 566
Carollo, C. M., Danziger, I. J., Rich, R. M., & Chen, X. 1997, ApJ, 491, 545
Chabrier, G. 2003, PASP, 115, 763
Coleman, G. D., Wu, C.-C., & Weedman, D. W. 1980, ApJS, 43, 393
Couch, W. J., & Sharples, R. M. 1987, MNRAS, 229, 423
de Jong, R. S. 1996, A&AS, 118, 557
Dressler, A., & Gunn, J. E. 1983, ApJ, 270, 7
Faber, S. M., & Jackson, R. E. 1976, ApJ, 204, 668
Ferreras, I., Wyse, R. F. G., & Silk, J. 2003, MNRAS, 345, 1381
Franx, M., Illingworth, G., & Heckman, T. 1989, ApJ, 344, 613
Freeman, K. C. 1970, ApJ, 160, 811
Geha, M., Guhathakurta, P., & van der Marel, R. P. 2003, AJ, 126, 1794
González Delgado, R. M., & Leitherer, C. 1999, ApJS, 125, 479
González Delgado, R. M., Leitherer, C., & Heckman, T. M. 1999, ApJS, 125, 489
Guzmán, R., Jangren, A., Koo, D. C., Bershady, M. A., & Simard, L. 1998, ApJ, 495, L13
Guzmán, R., Koo, D. C., Faber, S. M., Illingworth, G. D., Takamiya, M., Kron, R. G., & Bershady, M. A. 1996, ApJ, 460, L5
Guzmán, R., Östlin, G., Kunth, D., Bershady, M. A., Koo, D. C., & Pahre, M. A. 2003, ApJ, 586, L45
Guzmán, R., et al. 1997, ApJ, 489, 559
Halliday, C., Davies, R. L., Kuntschner, H., Birkinshaw, M., Bender, R., Saglia, R. P., & Baggley, G. 2001, MNRAS, 326, 473
Hammer, F., Gruel, N., Thuan, T., Flores, H., & Infante, L. 2001, ApJ, 550, 570
Homeier, N., Gallagher, J. S., III, & Pasquali, A. 2002, A&A, 391, 857
Homeier, N. L., & Gallagher, J. S. 1999, ApJ, 522, 199
Hoyos, C., Guzmán, R., Bershady, M. A., Koo, D. C., & Díaz, A. I. 2004, AJ, 128, 1541
Im, M., Faber, S. M., Gebhardt, K., Koo, D. C., Phillips, A. C., Schiavon, R. P., Simard, L., & Willmer, C. N. A. 2001, AJ, 122, 750
Impey, C., & Bothun, G. 1989, ApJ, 341, 89
Jerjen, H., Binggeli, B., & Freeman, K. C. 2000, AJ, 119, 593
Kobulnicky, H. A., & Gebhardt, K. 2000, AJ, 119, 1608

Kobulnicky, H. A, & Zaritsky, D. 1999, ApJ, 511, 118
Koo, D. C. 1986, ApJ, 311, 651
Koo, D. C., Bershady, M. A., Wirth, G. D., Stanford, A., & Majewski, S. R. 1994, ApJ, 427, L9
Koo, D. C., Guzman, R., Faber, S. M., Illingworth, G. D., Bershady, M. A., Kron, R. G., & Takamiya, M. 1995, ApJ, 440, L49
Koo, D. C., & Kron, R. G. 1988, ApJ, 325, 92
Koo, D. C., Kron, R. G., & Cudworth, K. M. 1986, PASP, 98, 285
Kormendy, J., & Kennicutt, R. C., Jr. 2004, ARA&A, 42, 603
Kron, R. G. 1980, ApJS, 43, 305
Magnier, E. A., & Cuillandre, J.-C. 2004, PASP, 116, 449
Majewski, S. R. 1992, ApJS, 78, 87
Majewski, S. R., Kron, R. G., Koo, D. C., & Bershady, M. A. 1994, PASP, 106, 1258
Martin, P., Savalle, R., Vermeulen, T., & Shapiro, J. N. 2002, Proc. SPIE, 4844, 74
Mateo, M. L. 1998, ARA&A, 36, 435
Munn, J. A., Koo, D. C., Kron, R. G., Majewski, S. R., Bershady, M. A., & Smetanka, J. J. 1997, ApJS, 109, 45
Newberry, M. V., Boroson, T. A., & Kirshner, R. P. 1990, ApJ, 350, 585
Norton, S. A., Gebhardt, K., Zabludoff, A. I., & Zaritsky, D. 2001, ApJ, 557, 150
Phillips, A. C., Guzman, R., Gallego, J., Koo, D. C., Lowenthal, J. D., Vogt, N. P., Faber, S. M., & Illingworth, G. D. 1997, ApJ, 489, 543
Pisano, D. J., Kobulnicky, H. A., Guzmán, R., Gallego, J., & Bershady, M. A. 2001, AJ, 122, 1194
Quintero, A. D., et al. 2004, ApJ, 602, 190
Rubin, V. C., Kenney, J. D. P., & Young, J. S. 1997, AJ, 113, 1250
Schweizer, F. 1996, AJ, 111, 109
Tremonti, C. A., et al. 2004, ApJ, 613, 898
Trevese, D., Kron, R. G., Majewski, S. R., Bershady, M. A., & Koo, D. C. 1994, ApJ, 433, 494
Trevese, D., Pittella, G., Koo, D. C., Kron, R. G., & Bershady, M. A. 1989, AJ, 98, 108
Vader, J. P., Vignoux, L., Lachièze-Rey, M., & Souviron, J. 1988, A&A, 203, 217
van Zee, L., Barton, E. J., & Skillman, E. D. 2004a, AJ, 128, 2797
van Zee, L., Skillman, E. D., & Haynes, M. P. 2004b, AJ, 128, 121
Yang, Y., Zabludoff, A. I., Zaritsky, D., Lauer, T. R., & Mihos, J. C. 2004, ApJ, 607, 258
Zabludoff, A. I., Zaritsky, D., Lin, H., Tucker, D., Hashimoto, Y., Shectman, S. A., Oemler, A., & Kirshner, R. P. 1996, ApJ, 466, 104